

Phenomenological study of a gauged $L_\mu - L_\tau$ model with a scalar leptoquark

Chuan-Hung Chen,^{1,2,*} Cheng-Wei Chiang^{3,2,†} and Chun-Wei Su^{3,‡}

¹*Department of Physics, National Cheng-Kung University, Tainan 70101, Taiwan*

²*Physics Division, National Center for Theoretical Sciences, Taipei 10617, Taiwan*

³*Department of Physics and Center for Theoretical Physics, National Taiwan University, Taipei 10617, Taiwan*

 (Received 8 September 2023; revised 5 January 2024; accepted 28 February 2024; published 21 March 2024)

A Z' gauge boson with sub-GeV mass has acquired a significant interest in phenomenology, particularly in view of the muon $g - 2$ anomaly and coherent elastic neutrino-nucleon scattering. The latter is challenged by the nuclear recoil energy of a few tens of keV but has been observed by the COHERENT experiment. To further reconcile the observed excesses in $R(D^{(*)})$ from semileptonic charmful B decays and in the W boson mass, we investigate a model with a gauged $U(1)_{L_\mu - L_\tau}$ symmetry and a scalar leptoquark. In contrast to the mechanism that involves kinetic mixing between the gauge bosons of $U(1)_{\text{em}}$ and $U(1)_{L_\mu - L_\tau}$, we adopt a dynamical symmetry breaking of $U(1)_{L_\mu - L_\tau}$ by incorporating an additional Higgs doublet. Through mixing with the $U(1)_{L_\mu - L_\tau}$ -charged Higgs doublet, new Higgs decay channels $h \rightarrow Z_1 Z_1 / Z_1 Z_2$ occur at percent-level branching ratios, which could be accessible at the LHC. The W -mass anomaly observed by CDF II can be potentially resolved through the enhancement in the oblique parameter T . Due to the flavored gauge symmetry, the introduced scalar leptoquark $S^\dagger = (\bar{3}, 1, 2/3)$ exhibits a unique coupling to the τ lepton, offering an explanation for the excesses observed in $R(D^{(*)})$. Moreover, $\tau \rightarrow \mu(Z_1 \rightarrow) e^- e^+$ via the resonant light gauge boson decay can reach the sensitivity of Belle II at an integrated luminosity of 50 ab^{-1} .

DOI: [10.1103/PhysRevD.109.055038](https://doi.org/10.1103/PhysRevD.109.055038)

I. INTRODUCTION

The possible existence of a sub-GeV Z' gauge boson has attracted much attention in recent years in addressing unresolved problems in particle physics phenomenology, particularly in flavor physics and dark matter (DM). The former includes the long-lasting puzzle in the anomalous magnetic dipole moment of muon (muon $g - 2$), while the latter could lead to establishing a portal between the visible and dark sectors.

Furthermore, a light Z' can play a substantial role in coherent elastic neutrino-nucleon scattering (CE ν NS). Since the proposal of measuring CE ν NS [1], conducting such experiments has been quite challenging, not just because of its tiny cross section but mostly due to the fact that the maximum nuclear recoil energy would be only several tens of keV. Nevertheless, the CE ν NS has finally

been observed by the COHERENT experiment using CsI and Ar targets [2–4]. The obtained total cross sections averaged over neutrino fluxes are

$$\begin{aligned} \langle \sigma \rangle_\phi &= (16.5_{-2.5}^{+3.0}) \times 10^{-39} \text{ cm}^2 [\text{Cs}], \\ \langle \sigma \rangle_\phi &= (2.2 \pm 0.7) \times 10^{-39} \text{ cm}^2 [\text{Ar}]. \end{aligned} \quad (1)$$

The standard model (SM) predictions are $18.9 \times 10^{-39} \text{ cm}^2$ [3] and $1.8 \times 10^{-39} \text{ cm}^2$ [4], respectively. Additionally, besides improving our understanding of atomic nuclei and neutrinos, precision measurements of CE ν NS can be used to explore or constrain physics beyond the SM [5–14]. Since the momentum transfer to the nucleus is at the sub-MeV level, a light Z' gauge boson stands out as one of the most appealing extensions of the SM [15–25].

Meanwhile, several deviations from the SM predictions have emerged in experiments, such as the muon $g - 2$, $R(D^{(*)})$ in the $B \rightarrow D^{(*)} \tau \bar{\nu}$ decays and the mass of W gauge boson. It would be intriguing to build a light Z' model that cannot only resolve these observed anomalies but also have a significant impact on the CE ν NS phenomenon. To fulfill these objectives within one coherent framework, we consider extending the SM with a new local $U(1)$ gauge symmetry. Numerous potential candidates of such a $U(1)$

*physchen@mail.ncku.edu.tw

†chengwei@phys.ntu.edu.tw

‡r10222026@ntu.edu.tw

Published by the American Physical Society under the terms of the Creative Commons Attribution 4.0 International license. Further distribution of this work must maintain attribution to the author(s) and the published article's title, journal citation, and DOI. Funded by SCOAP³.

gauge symmetry exist in the literature, including universal $U(1)$, $B - L$, $B_y + L_\mu + L_\tau$, $B - 3L_\ell$, $B - L_e - 2L_\mu$, and $L_{\ell-\ell'}$ [25], where B_i and L_ℓ denote the quantum numbers of quark and lepton, respectively. Among these, we find that in addition to satisfying gauge anomaly-free conditions without introducing new chiral fermions, the gauged $U(1)_{L_\mu-L_\tau} \equiv U(1)_{\mu-\tau}$ model can effectively address the above-mentioned concerns.

Having $U(1)_{\mu-\tau}$ symmetry as a gauge extension of the SM has many advantages from a phenomenological viewpoint [26,27]. As mentioned earlier, the gauge coupling $g_{Z'}$ of $\mathcal{O}(10^{-4})$ with Z' mass of $\mathcal{O}(10-200)$ MeV can explain muon $g-2$ [28], where the discrepancy between experimental measurements and theoretical calculations, which use the data-driven approach to evaluate the hadronic vacuum polarization, reaches $\sim 4\sigma$ [29]:

$$\Delta a_\mu = a_\mu^{\text{exp}} - a_\mu^{\text{SM}} = (2.51 \pm 0.59) \times 10^{-9}. \quad (2)$$

Instead of kinetic mixing between $U(1)_{\text{em}}$ and $U(1)_{\mu-\tau}$ [16,20,25], we examine the $Z' - Z$ mass mixing scenario, which arises from the consideration of spontaneous $U(1)_{\mu-\tau}$ symmetry breakdown by a new scalar field carrying the $U(1)_{\mu-\tau}$ charge [28,30]. It would be useful if the new scalar field could also resolve any potential anomalies from a phenomenological perspective. Interestingly, the CDF II Collaboration used the full dataset from proton-antiproton collisions at $\sqrt{s} = 1.96$ TeV to determine the mass of the W boson as [31]

$$m_W = 80.4335 \pm 0.0094 \text{ GeV}. \quad (3)$$

The newly observed value differs from earlier measurements of $m_W = 80.385 \pm 0.015$ GeV from the combined results of LEP and Tevatron [32] and $m_W = 80.360 \pm 0.016$ GeV from the updated ATLAS result [33]. Moreover, it deviates from the SM prediction of $m_W = 80.361$ GeV [34] by $\sim 7\sigma$. If the anomaly in the W -mass measurement is confirmed with more data from the LHC, it would provide another piece of strong evidence for new physics. [35–53]. This anomaly also motivates the introduction of a Higgs doublet charged under the $U(1)_{\mu-\tau}$ symmetry [54,55].

The observed anomalies in the ratio of branching ratios (BRs) in semileptonic charmed B decays are defined by

$$R(M) = \frac{\text{BR}(B \rightarrow M\tau\bar{\nu})}{\text{BR}(B \rightarrow M\ell\bar{\nu})}, \quad (4)$$

with $M = D, D^*$. The SM predictions are $R(D) = 0.298 \pm 0.004$ and $R(D^*) = 0.254 \pm 0.005$ [56–63], while the current experimental values are $R(D) = 0.356 \pm 0.029$ and $R(D^*) = 0.284 \pm 0.013$ [64]. Recent measurements from LHCb have been included in the average [65,66].

As seen, there is an overall 3.3σ deviation from the SM predictions [64]. Because $B \rightarrow M\tau\bar{\nu}$ is mediated by the tree-level charged weak currents in the SM, the required mechanism to enhance $R(M)$ should have nonuniversal lepton couplings and be induced at the tree level. Although $R(J/\Psi)$ and $R(\Lambda_c)$ have the potential to observe the breakdown of lepton universality as well, their statistical errors in the experimental data are still too large to be conclusive [67–69]. Hence, we concentrate solely on $R(D)$ and $R(D^*)$ in this work.

Without further introducing a heavy charged gauge boson (e.g., W') or vector leptoquark (LQ) for the $R(D^{(*)})$ anomalies, the new mediating bosons of interest include a charged Higgs boson [70–75] and a scalar LQ [76–83]. The flavored $U(1)_{\mu-\tau}$ symmetry strictly limits the Yukawa couplings to different lepton flavors, resulting in a suppressed contribution of the charged Higgs to $R(M)$ by $m_b m_\tau / v^2$ in this model, where v is the combined vacuum expectation value (VEV) of the introduced Higgs doublets. Hence, the introduction of scalar LQ emerges as a more apposite solution. We find that among various LQ representations, the simplest choice to explain the observed excess in $R(M)$ is the $S^{\frac{1}{3}} = (\bar{3}, 1, 2/3)$ representation under the $SU(3)_C \times SU(2)_L \times U(1)_Y$ gauge symmetries. Additionally, based on the flavored $U(1)_{\mu-\tau}$ gauge symmetry, there is a natural suppression in the LQ Yukawa couplings to the light leptons, while the τ lepton and τ neutrino, respectively couple to up- and down-type quarks to resolve the observed anomaly in $R(M)$. It is worth mentioning that using the exclusive- and hadronic-tag approaches with 362 fb^{-1} of data, the Belle II Collaboration recently has observed the first evidence of $B^+ \rightarrow K^+ \nu \bar{\nu}$ decay with a 2.7σ deviation from the SM prediction, and the measured result is given as $\text{BR}(B^+ \rightarrow K^+ \nu \bar{\nu}) = (2.3 \pm 0.5_{-0.4}^{+0.5}) \times 10^{-5}$ [84]. Applying the LQ $S^{\frac{1}{3}}$ in the model, the branching ratios for $B \rightarrow (K, K^*) \nu_\tau \bar{\nu}_\tau$ can be significantly enhanced. A detailed phenomenological analysis of the neutrino-pair production in B and K meson decays can be found in Ref. [85].

In addition to the total cross section of $\text{CE}\nu\text{NS}$ and $R(D^{(*)})$, we propose new observables sensitive to new physics as a function of incident neutrino energy for elastic neutrino-nucleus scattering and as a function of invariant mass-square q^2 of $\ell\nu$ for semileptonic charmed B decays. We find that $\text{CE}\nu\text{NS}$ mediated by the light physical Z_1 can deviate significantly from the SM in the low neutrino energy regime. Additionally, $R(D)$ in the large q^2 regime is more sensitive to the leptoquark effects and can significantly differ from the SM.

This paper is organized as follows: In Sec. II, we formulate the model and derive the spectrum of scalar bosons and various new couplings. The $Z' - Z$ mixing and lepton flavor mixing are also discussed in detail. With the new interactions, Sec. III discusses the new physics effects on various phenomena, including the cross section of

CE ν NS, values of $R(D)$ and $R(D^*)$, new Higgs decay channels $h \rightarrow HH/Z_1Z_1/Z_1Z_2$, LFV processes, lepton $g-2$, and the oblique parameters. Constraints on the model parameters and detailed numerical analysis are presented in Sec. IV. A summary of our findings is given in Sec. V.

II. THE MODEL

We consider in this work a model that extends the SM gauge symmetry by the $U(1)_{\mu-\tau}$ gauge symmetry, under which only the μ and τ leptons in the SM are charged. Due to the opposite $U(1)_{\mu-\tau}$ charges within the second and third generations of leptons, it can be easily checked that the loop-induced triangle anomalies mediated by the muon and τ lepton for $U(1)_{\mu-\tau}^3$, $U(1)_{\mu-\tau}^2 U(1)_Y$, $U(1)_{\mu-\tau} U(1)_Y^2$, $SU(2)^2 U(1)_{\mu-\tau}$, and gravity 2 - $U(1)_{\mu-\tau}$ cancel out automatically without the need of introducing extra chiral fermions. As a result, the gauged $U(1)_{\mu-\tau}$ symmetry model stands free from gauge anomalies.

In addition to the SM Higgs doublet, denoted by H_2 , whose neutral component has a VEV, v_2 , to spontaneously break $SU(2)_L \times U(1)_Y$, we introduce an additional Higgs doublet, denoted by H_1 , which carries not only the $U(1)_{\mu-\tau}$ charge, twice that of μ , but also the weak isospin and $U(1)_Y$ hypercharge. The new Higgs doublet is assumed to also develop a VEV, v_1 , in its neutral component to break $U(1)_{\mu-\tau}$ besides $SU(2)_L \times U(1)_Y$, resulting in a massive Z' boson. Therefore, unlike the conventional two-Higgs-doublet model (2HDM), the model has one charged Higgs and two CP -even Higgs bosons but has no CP -odd Higgs boson, as it has become the longitudinal component of Z' . Finally, we include an $SU(2)_L$ -singlet scalar LQ with hypercharge $Y = 2/3$ that also has the same $U(1)_{\mu-\tau}$ charge as μ . The quantum number assignments of the leptons, the Higgs doublets, and the LQ are given in Table I. As we will see, such a model can simultaneously accommodate the measured lepton $g-2$, $R(D^*)$, and W mass anomalies, while the cross section of the CE ν NS process can be enhanced to deviate from the SM expectation by up to 25%.

In the following subsections, we analyze the spectra of Higgs and gauge bosons and determine their physical eigenstates. In addition, we also derive the gauge, Yukawa, and trilinear couplings of Higgs bosons, which

TABLE I. Quantum numbers of the leptons, Higgs doublets, and scalar leptoquark.

	$e_{L(R)}$	$\mu_{L(R)}$	$\tau_{L(R)}$	H_2	H_1	S^\dagger
$L_\mu - L_\tau$	0	q_X	$-q_X$	0	$2q_X$	q_X
$SU(2)_L$	2(1)	2(1)	2(1)	2	2	1
$U(1)_Y$	$-1(-2)$	$-1(-2)$	$-1(-2)$	1	1	$2/3$

are used for the phenomenological analysis presented in the paper.

A. Spectra of Higgs bosons and Higgs-related trilinear couplings

We first write down the scalar potential consistent with the $SU(2)_L \times U(1)_Y \times U(1)_{\mu-\tau}$ gauge symmetry as

$$\begin{aligned} V(H_1, H_2, S^\dagger) = & \mu_1^2 H_1^\dagger H_1 + \mu_2^2 H_2^\dagger H_2 + \frac{\lambda_1}{2} (H_1^\dagger H_1)^2 \\ & + \frac{\lambda_2}{2} (H_2^\dagger H_2)^2 + \lambda_3 H_1^\dagger H_1 H_2^\dagger H_2 \\ & + \lambda_4 H_1^\dagger H_2 H_2^\dagger H_1 + \mu_5^2 S^{-\frac{1}{3}} S^\dagger \\ & + S^{-\frac{1}{3}} S^\dagger (\lambda_1^S H_1^\dagger H_1 + \lambda_2^S H_2^\dagger H_2). \end{aligned} \quad (5)$$

Owing to the $U(1)_{\mu-\tau}$ symmetry, there is no so-called μ term that couples $H_{1,2}$ quadratically, and all terms in Eq. (5) are self-Hermitian due to the $U(1)_{\mu-\tau}$ symmetry, rendering all the coefficients real. The components of two Higgs doublets can be parametrized as ($i = 1, 2$)

$$H_i = \begin{pmatrix} \phi^+ \\ \frac{1}{\sqrt{2}}(v_i + \phi_i^0 + i\eta_i) \end{pmatrix}. \quad (6)$$

Using the tadpole conditions $\partial V / \partial v_{i,2} = 0$, we obtain two equalities:

$$\begin{aligned} \mu_1^2 + \frac{\lambda_1}{2} v_1^2 + \frac{\lambda_{34}}{2} v_2^2 &= 0, \\ \mu_2^2 + \frac{\lambda_2}{2} v_2^2 + \frac{\lambda_{34}}{2} v_1^2 &= 0, \end{aligned} \quad (7)$$

with $\lambda_{34} \equiv \lambda_3 + \lambda_4$. To achieve spontaneous breakdown of the $SU(2)_L \times U(1)_Y \times U(1)_{\mu-\tau}$ gauge symmetry, we require $\mu_{1,2}^2 < 0$. For the vacuum stability, where the scalar potential is bounded from below in all field configurations, the quartic couplings have to satisfy the criteria given by [86,87]

$$\lambda_{1,2} \geq 0, \quad \lambda_3 + \sqrt{\lambda_1 \lambda_2} \geq 0, \quad \lambda_{34} + \sqrt{\lambda_1 \lambda_2} \geq 0. \quad (8)$$

Two neutral Goldstone bosons result from the mixing between the two CP -odd components:

$$\begin{pmatrix} G_{Z'}^0 \\ G_Z^0 \end{pmatrix} = \begin{pmatrix} c_\beta & s_\beta \\ -s_\beta & c_\beta \end{pmatrix} \begin{pmatrix} \eta_1 \\ \eta_2 \end{pmatrix} \equiv U_\beta \begin{pmatrix} \eta_1 \\ \eta_2 \end{pmatrix}, \quad (9)$$

where β is defined by $t_\beta \equiv \tan \beta = v_2 / v_1$, $v = \sqrt{v_1^2 + v_2^2}$, $c_\beta \equiv \cos \beta$, and $s_\beta \equiv \sin \beta$. To obtain the states of charged Goldstone and charged Higgs bosons, we can use Eq. (9) by substituting (G^\pm, H^\pm) and (ϕ_1^\pm, ϕ_2^\pm) for $(G_{Z'}^0, G_Z^0)$ and (η_1, η_2) , respectively. As a result, the mass squared of the

charged Higgs boson is solely dependent on the parameter λ_4 as follows:

$$m_{H^\pm}^2 = -\frac{\lambda_4}{2}v^2. \quad (10)$$

Since the massive LQ is irrelevant to the EWSB, its mass squared with the assumption that $\mu_S^2 > 0$ is found to be

$$m_S^2 = \mu_S^2 + \frac{v^2}{2}(\lambda_1^S c_\beta^2 + \lambda_2^S s_\beta^2), \quad (11)$$

and can be as heavy as $\mathcal{O}(\text{TeV})$.

From the scalar potential in Eq. (5) and the tadpole conditions in Eq. (7), the mass terms for the CP -even scalars can be written as

$$\frac{1}{2}(\phi_1^0, \phi_2^0) \begin{pmatrix} \lambda_1 v_1^2 & v_1 v_2 \lambda_{34} \\ v_1 v_2 \lambda_{34} & \lambda_2 v_2^2 \end{pmatrix} \begin{pmatrix} \phi_1^0 \\ \phi_2^0 \end{pmatrix}. \quad (12)$$

Equation (12) can be diagonalized by a 2×2 orthogonal matrix, and the resulting eigenstates of neutral Higgses can be parametrized using a mixing angle α as

$$\begin{pmatrix} H \\ h \end{pmatrix} = \begin{pmatrix} c_\alpha & s_\alpha \\ -s_\alpha & c_\alpha \end{pmatrix} \begin{pmatrix} \phi_1^0 \\ \phi_2^0 \end{pmatrix} \equiv U_\alpha \begin{pmatrix} \phi_1^0 \\ \phi_2^0 \end{pmatrix}, \quad (13)$$

where h is the 125-GeV SM-like Higgs boson, $c_\alpha \equiv \cos \alpha$, and $s_\alpha \equiv \sin \alpha$. In the following, we would focus on the scenario where the new CP -even state is lighter than the SM-like Higgs boson, i.e., $m_h > m_H$. Using the parameters λ_i and v_i , the masses of the h and H states, as well as the mixing angle between them, can be obtained as

$$m_{h,H}^2 = \frac{\lambda_1 v_1^2 + \lambda_2 v_2^2}{2} \pm \frac{1}{2} \sqrt{(\lambda_1 v_1^2 - \lambda_2 v_2^2)^2 + 4v_1^2 v_2^2 \lambda_{34}^2},$$

$$\tan 2\alpha = -\frac{2v_1 v_2 \lambda_{34}}{\lambda_2 v_2^2 - \lambda_1 v_1^2}. \quad (14)$$

The scalar potential in the model involves six parameters, namely, $\mu_{1,2}^2$ and λ_{1-4} . One can write them in terms of the physical parameters $\{m_{H^\pm, h, H}, v, \alpha, \beta\}$ as

$$\mu_1^2 = -\frac{1}{2c_\beta}(-s_\alpha s_{\beta-\alpha} m_h^2 + c_\alpha c_{\beta-\alpha} m_H^2), \quad (15a)$$

$$\mu_2^2 = -\frac{1}{2s_\beta}(c_\alpha s_{\beta-\alpha} m_h^2 + s_\alpha c_{\beta-\alpha} m_H^2), \quad (15b)$$

$$\lambda_1 = \frac{1}{v^2 c_\beta^2}(m_h^2 s_\alpha^2 + m_H^2 c_\alpha^2), \quad (15c)$$

$$\lambda_2 = \frac{1}{v^2 s_\beta^2}(m_h^2 c_\alpha^2 + m_H^2 s_\alpha^2), \quad (15d)$$

$$\lambda_3 = -\frac{s_{2\alpha}}{v^2 s_{2\beta}}(m_h^2 - m_H^2) + \frac{2m_{H^\pm}^2}{v^2}, \quad (15e)$$

$$\lambda_4 = -\frac{2m_{H^\pm}^2}{v^2}. \quad (15f)$$

An important parameter of the scalar potential in the SM is the quartic coupling λ_{SM} , which not only determines the mass of the SM Higgs boson via $m_h^2 = \lambda_{\text{SM}} v^2$ but also controls the potential shape. Therefore, to probe the existence of extra scalars, it becomes crucial to precisely determine the Higgs self-coupling through the hh production that involves the Higgs trilinear coupling [88]. In the 2HDM, the SM-like Higgs field is a linear combination of $\phi_{1,2}^0$, and, instead of a factor of $3m_h^2/v$ for the SM, the Higgs self-coupling also involves the parameters β and α . Moreover, when $m_H < m_h/2$, the decay channel $h \rightarrow HH$ becomes accessible. Current measurements of Higgs decays can impose stringent constraints on the related parameters. To take these constraints into account, we present all the Higgs trilinear couplings as follows:

$$\begin{aligned} -\mathcal{L} \supset & -\frac{s_{2\alpha} s_{\beta-\alpha}}{v s_{2\beta}}(m_h^2 + 2m_H^2) \frac{hH^2}{2} \\ & + \frac{s_{2\alpha} c_{\beta-\alpha}}{v s_{2\beta}}(2m_h^2 + m_H^2) \frac{h^2 H}{2} \\ & + \frac{3m_h^2}{v} \left(s_{\beta-\alpha} + \frac{2}{s_{2\beta}} c_{\beta+\alpha} c_{\beta-\alpha}^2 \right) \frac{h^3}{3!} \\ & + \frac{3m_H^2}{v} \left(c_{\beta-\alpha} + \frac{2}{s_{2\beta}} s_{\beta+\alpha} s_{\beta-\alpha}^2 \right) \frac{H^3}{3!} \\ & + v(\lambda_+^S c_{\beta-\alpha} + \lambda_-^S c_{\beta+\alpha}) H S^{-\frac{1}{3}} S^{\frac{1}{3}} \\ & + v(\lambda_+^S s_{\beta-\alpha} - \lambda_-^S s_{\beta+\alpha}) h S^{-\frac{1}{3}} S^{\frac{1}{3}}. \end{aligned} \quad (16)$$

Taking the limits of $\alpha \rightarrow 0$ and $s_\beta \rightarrow 1$, it can be seen that only the self-couplings of h and H remain. We note that the scalar couplings to the LQ are also included, which can be used to analyze the loop-induced Higgs boson decays.

B. Z' – Z mixing and gauge couplings of scalars

The masses of the gauge bosons and the gauge couplings of scalars are determined by the kinetic terms of $H_{1,2}$, with the covariant derivatives given as

$$D_\mu H_1 = \left(\partial_\mu + i\frac{g}{2} \vec{\tau} \cdot \vec{W}_\mu + i\frac{g'}{2} B_\mu + g_{Z'} X Z'_\mu \right) H_1,$$

$$D_\mu H_2 = \left(\partial_\mu + i\frac{g}{2} \vec{\tau} \cdot \vec{W}_\mu + i\frac{g'}{2} B_\mu \right) H_2,$$

$$D_\mu S^{\frac{1}{3}} = \left(\partial_\mu + iQ_S g' B_\mu + i g_{Z'} q_X Z'_\mu \right) S^{\frac{1}{3}}, \quad (17)$$

where g , g' , and $g_{Z'}$ denote the gauge couplings of $SU(2)_L$, $U(1)_Y$, and $U(1)_{\mu-\tau}$, respectively, $X = 2q_X$ is the $U(1)_{\mu-\tau}$

charge of H_1 , and $Q_S = 1/3$ is the electric charge of LQ. As in the conventional 2HDM, the tree-level W boson mass can be obtained as $m_W = gv/2$. However, since H_1 carries the charges of both electroweak and $U(1)_{\mu-\tau}$ symmetries, its VEV breaks not only $SU(2)_L \times U(1)_Y$ but also $U(1)_{\mu-\tau}$ at the same time. As a result, the Z and Z' states are not physical and generally mix with each other. More explicitly, the mass squared terms for Z and Z' are given by

$$\frac{1}{2} \begin{pmatrix} Z' & Z \end{pmatrix} \begin{pmatrix} m_{Z'}^2 & m_{Z'Z}^2 \\ m_{Z'Z}^2 & m_Z^2 \end{pmatrix} \begin{pmatrix} Z' \\ Z \end{pmatrix}, \quad (18)$$

where $m_{Z'}^2$, m_Z^2 , and $m_{Z'Z}^2$ are defined as

$$\begin{aligned} m_{Z'}^2 &= g_{Z'}^2 X^2 v_1^2 = \frac{(g_{Z'} X v)^2}{1 + t_\beta^2}, \\ m_Z^2 &= \frac{g^2 + g'^2}{4} v^2 = \frac{g^2 v^2}{4} (1 + t_W^2), \\ m_{Z'Z}^2 &= -\frac{gg_{Z'} X}{2c_W} v_1^2 = -\frac{gg_{Z'} X v^2}{2c_W (1 + t_\beta^2)}. \end{aligned} \quad (19)$$

The states of the photon and Z boson fields are written, as in the SM, as

$$\begin{aligned} A_\mu &= c_W B_\mu + s_W W_\mu^3, \\ Z_\mu &= -s_W B_\mu + c_W W_\mu^3, \end{aligned} \quad (20)$$

where $c_W \equiv \cos \theta_W$, $s_W \equiv \sin \theta_W$, and θ_W is the weak mixing angle. The mass squared matrix in Eq. (18) can be diagonalized using a 2×2 orthogonal matrix, parametrized by a mixing angle θ_Z , in a fashion analogous to Eq. (13). Assuming that $m_{Z'} \ll m_Z$ and taking Z_1 and Z_2 as the physical states of the neutral gauge bosons, their mass squares and mixing angle can be approximately obtained as follows:

$$\begin{aligned} m_{Z_1}^2 &\simeq m_{Z'}^2 - \frac{m_{Z'Z}^4}{m_Z^2} = m_{Z'}^2 \frac{t_\beta^2}{1 + t_\beta^2}, \\ m_{Z_2}^2 &\simeq m_Z^2 + \frac{m_{Z'Z}^4}{m_Z^2}, \\ s_{\theta_Z} &\simeq -\text{sign}(\theta_Z) \frac{m_{Z'Z}^2}{m_Z^2} = \text{sign}(\theta_Z) \frac{2c_W m_{Z_1}}{gt_\beta v}, \end{aligned} \quad (21)$$

where $\text{sign}(\theta_Z) = \pm 1$ represents the sign of the mixing angle. Apparently, the mixing angle is suppressed by $m_{Z_1}/(vt_\beta)$ as t_β gets large. If the mass of m_{Z_1} is of $\mathcal{O}(10)$ MeV, s_{θ_Z} is at most of $\mathcal{O}(10^{-5})$.

To study the loop-induced processes or variables (e.g., lepton $g-2$) mediated by the Z_1 boson, we also need the gauge couplings of scalars and LQ as follows:

$$\begin{aligned} \mathcal{L} \supset & i \frac{g}{2c_W} [(\partial^\mu H^-)H^+ - H^- \partial^\mu H^+] (s_{2W} A_\mu + c_{2W} Z_\mu) \\ & + \left[-i \frac{g_{S\beta-\alpha}}{2} W_\mu^+ (H \partial^\mu H^- - H^- \partial^\mu H) \right. \\ & + i \frac{g_{C\beta-\alpha}}{2} W_\mu^+ (h \partial^\mu H^- - H^- \partial^\mu h) + \text{H.c.} \left. \right] \\ & + g m_W W_\mu^- W^{+\mu} (s_{\beta-\alpha} h + c_{\beta-\alpha} H) \\ & - i Q_S e (A_\mu - t_W Z_\mu) (S^{-\frac{1}{3}} \partial^\mu S^{\frac{1}{3}} - S^{\frac{1}{3}} \partial^\mu S^{-\frac{1}{3}}) \\ & + \frac{2m_Z^2}{v} (c_{\beta-\alpha} H + s_{\beta-\alpha} h) \frac{Z_\mu Z^\mu}{2} + \frac{2m_{Z'}^2}{v_1} (c_\alpha H - s_\alpha h) \frac{Z'_\mu Z'^\mu}{2} \\ & - \frac{g m_{Z'}}{c_W} (c_\alpha H - s_\alpha h) Z'_\mu Z^\mu. \end{aligned} \quad (22)$$

C. Yukawa couplings of fermions

The Yukawa sector plays a crucial role in flavor physics as it governs the mass generation of the SM fermions and the couplings of scalars to fermions in the model. The Lagrangian of the Yukawa sector under $SU(2)_L \times U(1)_Y \times U(1)_{\mu-\tau}$ gauge symmetry can be written based on the quantum number assignments in Table I as

$$\begin{aligned} -\mathcal{L}_Y &= \overline{Q}_L H_2 \mathbf{Y}^d d_R + \overline{Q}_L \tilde{H}_2 \mathbf{Y}^u u_R + \overline{L}_\ell H_2 \mathbf{Y}^\ell \ell_R \\ & + y_{\mu\tau} \overline{L}_\mu H_1 \tau_R + \overline{Q}_L^c i \tau_2 \mathbf{Y}_L^q L_\tau S^{\frac{1}{3}} + \overline{u}_R^c \mathbf{Y}_R^u \tau_R S^{\frac{1}{3}} + \text{H.c.}, \end{aligned} \quad (23)$$

where, except for the $\overline{L}_\mu H_1 \tau_R$ term, the flavor indices are all suppressed, $Q_L^T = (u, d)_L^T$ and $L^T = (\nu_\ell, \ell)_L^T$ represent the quark and lepton doublets, respectively, ℓ_R denotes the right-handed charged lepton, and $F^c = C\gamma^0 F^*$ for a fermion F with C being the charge conjugation operator. The $U(1)_{\mu-\tau}$ gauge symmetry restricts the 3×3 Yukawa matrix \mathbf{Y}^ℓ to be a diagonal matrix; i.e., $\mathbf{Y}^\ell = \text{diag}(y^\ell, y^\mu, y^\tau)$. We note that because H_1 and H_2 simultaneously couple to the charged leptons, the term $\overline{L}_\mu H_1 \tau_R$ will induce flavor-changing neutral currents (FCNCs) at tree level. After diagonalizing the quark mass matrices and using the physical states of scalars, the Yukawa couplings of quarks to $h(H)$ and H^\pm are found to be the same as those in type-I 2HDM [89]. Although the charged Higgs boson could in principle enhance the $b \rightarrow c\tau\nu$ transition [70–75], the involved Yukawa couplings in this model are suppressed by $m_{b,c}/(\tan\beta\sqrt{v_1^2 + v_2^2})$ and are irrelevant for our later discussions. The explicit expressions of the couplings can be found in Ref. [89].

While the diagonal \mathbf{Y}^ℓ matrix contributes to the charged lepton masses, the $\overline{L}_\mu H_1 \tau_R$ term induces flavor mixing between the μ and τ leptons. Thus, the electron mass is

simply $m_e = y^e v_2/\sqrt{2}$, and the mass matrix for the μ and τ leptons is expressed as

$$(\bar{\mu}_L, \bar{\tau}_L)\mathbf{M}_\ell \begin{pmatrix} \mu_R \\ \tau_R \end{pmatrix} = (\bar{\mu}_L, \bar{\tau}_L) \begin{pmatrix} \hat{m}_\mu & \hat{m}_{\mu\tau} \\ 0 & \hat{m}_\tau \end{pmatrix} \begin{pmatrix} \mu_R \\ \tau_R \end{pmatrix}, \quad (24)$$

where $\hat{m}_{\mu(\tau)} = y^{\mu(\tau)} v_2/\sqrt{2}$ and $\hat{m}_{\mu\tau} = y_{\mu\tau} v_1/\sqrt{2}$. The matrix \mathbf{M}_ℓ can be diagonalized through a bi-unitary transformation: $\mathbf{m}_\ell = V_L^\ell \mathbf{M}_\ell V_R^{\ell\dagger}$. Accordingly, the Yukawa couplings of the Higgs bosons to the leptons are found to be

$$\begin{aligned} -\mathcal{L}_Y \supset & \bar{\ell}_L \mathbf{m}_\ell \ell_R + \bar{\ell}_L \frac{\mathbf{m}_\ell}{v} \ell_R \left(\frac{c_\alpha}{s_\beta} h + \frac{s_\alpha}{s_\beta} H \right) \\ & + \bar{\ell}_L \frac{\mathbf{X}_\ell}{v} \ell_R \left(-\frac{2c_{\beta-\alpha}}{s_{2\beta}} h + \frac{2s_{\beta-\alpha}}{s_{2\beta}} H \right) \\ & + \bar{\nu}_L \left(\frac{\sqrt{2}\mathbf{m}_\ell}{vt_\beta} - \frac{2\sqrt{2}\mathbf{X}_\ell}{s_{2\beta}v} \right) \ell_R H^+ + \text{H.c.}, \quad (25) \end{aligned}$$

where \mathbf{X}_ℓ is defined as

$$\mathbf{X}_\ell = V_L^\ell \begin{pmatrix} 0 & \hat{m}_{\mu\tau} \\ 0 & 0 \end{pmatrix} V_R^{\ell\dagger}. \quad (26)$$

It is worth mentioning that \mathbf{X}_ℓ induces the tree-level FCNCs mediated by the Higgs bosons in the lepton sector. To see the decoupling and large $\tan\beta$ limits, it is useful to rewrite c_α/s_β and s_α/s_β as

$$\begin{aligned} \frac{c_\alpha}{s_\beta} &= s_{\beta-\alpha} + t_\beta^{-1} c_{\beta-\alpha}, \\ \frac{s_\alpha}{s_\beta} &= c_{\beta-\alpha} - t_\beta^{-1} s_{\beta-\alpha}. \quad (27) \end{aligned}$$

When the lepton Yukawa couplings are real, we can obtain the 2×2 flavor mixing matrices $V_{R,L}^\ell$ using the identities:

$$\begin{aligned} \mathbf{m}_\ell^\dagger \mathbf{m}_\ell &= V_R^\ell \mathbf{M}_\ell^\dagger \mathbf{M}_\ell V_R^{\ell\dagger}, \\ \mathbf{m}_\ell \mathbf{m}_\ell^\dagger &= V_L^\ell \mathbf{M}_\ell \mathbf{M}_\ell^\dagger V_L^{\ell\dagger}. \quad (28) \end{aligned}$$

By parametrizing $V_{R,L}^\ell$ in the same form as U_α in Eq. (13), we can obtain the mixing angles $\theta_{R,L}$ as

$$\begin{aligned} \tan 2\theta_R &= -\frac{2\hat{m}_\mu \hat{m}_{\mu\tau}}{\hat{m}_\tau^2 + \hat{m}_{\mu\tau}^2 - \hat{m}_\mu^2}, \\ \tan 2\theta_L &= -\frac{2\hat{m}_\tau \hat{m}_{\mu\tau}}{\hat{m}_\tau^2 - \hat{m}_{\mu\tau}^2 - \hat{m}_\mu^2}. \quad (29) \end{aligned}$$

In the limit when $\hat{m}_\mu \hat{m}_{\mu\tau}/\hat{m}_\tau^2$ is negligible, these mixing angles can be obtained to a good approximation as

$$\theta_R \approx 0, \quad s_{\theta_L} \simeq -\hat{m}_{\mu\tau}/\hat{m}_\tau. \quad (30)$$

As a free parameter with the mass dimension that appears only in the $\mu - \tau$ element of \mathbf{X}_ℓ , $\hat{m}_{\mu\tau}$ can be parametrized in terms of a free parameter $\chi_{\mu\tau}$ as $\hat{m}_{\mu\tau} = \chi_{\mu\tau} \sqrt{m_\mu m_\tau}$, where $m_{\mu,\tau}$ are the physical masses of μ and τ leptons. Using the approximate mixing angles in Eq. (30), we obtain

$$\begin{aligned} \hat{m}_\mu^2 &\simeq m_\mu^2 \left(1 - \chi_{\mu\tau}^2 \frac{m_\mu}{m_\tau} \right) \approx m_\mu^2, \\ \hat{m}_\tau^2 &\simeq m_\tau^2 \left(1 - \chi_{\mu\tau}^2 \frac{m_\mu}{m_\tau} \right), \\ \mathbf{X}_\ell &\simeq \begin{pmatrix} 0 & \chi_{\mu\tau} \sqrt{m_\mu m_\tau} \\ 0 & \chi_{\mu\tau}^2 m_\mu \end{pmatrix}. \quad (31) \end{aligned}$$

We now discuss the LQ couplings to quarks and leptons. Since the Yukawa couplings \mathbf{y}_L^q and \mathbf{y}_R^u are free parameters, the up-type quark flavor mixings can be absorbed into these parameters. As such, the up-type quark fields appearing in the LQ couplings in Eq. (23) can be treated as the physical states. However, the same \mathbf{y}_L^q also appears in the couplings to the down-type quarks. Therefore, in addition to V_L^d , the LQ couplings to the down-type quarks must include V_L^u . With $V_R^\ell \simeq \mathbb{1}$ and $V_{\text{CKM}} = V_L^u V_L^{d\dagger}$, we can express the Yukawa couplings of the LQ as

$$\begin{aligned} -\mathcal{L}_Y \supset & \left(\bar{u}_L^c \mathbf{y}_L^q V_{L\tau\ell}^{\ell\dagger} P_L \ell + \bar{u}_R^c \mathbf{y}_R^u P_R \tau \right) S^{\frac{1}{2}} \\ & - \bar{d}_L^c V_{\text{CKM}}^T \mathbf{y}_L^q P_L \nu_\tau S^{\frac{1}{2}} + \text{H.c.} \quad (32) \end{aligned}$$

D. Gauge couplings of fermions

Next, we consider the gauge couplings of the fermions. Since the $U(1)_{\mu-\tau}$ gauge symmetry does not affect the weak charged currents, they remain the same as those in the SM. Although quarks do not carry the $U(1)_{\mu-\tau}$ charge and thus do not directly couple to the Z' gauge boson, their couplings to the Z' boson can be induced through the mixing with the SM Z boson. Intriguingly, the distinct $U(1)_{\mu-\tau}$ charges carried by the muon and tau lepton lead to a lepton FCNC in the interaction $\bar{\mu}_L \gamma^\mu \tau_L Z'_\mu$. Due to the $Z' - Z$ mixing, they then result in Z -mediated lepton FCNCs although such effects are suppressed by $s_{\theta_L} s_{\theta_Z}$. Using the results shown in Eqs. (21) and (30) for the lepton-flavor and $Z' - Z$ mixings, respectively, we obtain the neutral gauge couplings to fermions as follows:

$$\begin{aligned} \mathcal{L}_{f f V}^N &= -\sum_f Q_f e \bar{f} \gamma^\mu f A_\mu - \frac{g}{2c_W} \sum_f \bar{f} \gamma^\mu (C_{iV}^f - C_{iA}^f \gamma_5) f Z_{i\mu} \\ &+ [g_{Z'} q_X s_{2\theta_L} \bar{\mu}_L \gamma^\mu \tau_L (c_{\theta_Z} Z_{1\mu} - s_{\theta_Z} Z_{2\mu}) + \text{H.c.}], \quad (33) \end{aligned}$$

where the coefficients $C_{iV,iA}^f$ are explicitly given by

$$\begin{aligned} C_{1V}^f &= c_V^f s_{\theta_Z} + \frac{c_W m_{Z_1} c_{\theta_Z}}{g v} X_V^f \sqrt{2 + t_\beta^2 + t_\beta^{-2}}, \\ C_{1A}^f &= c_A^f s_{\theta_Z} + \frac{c_W m_{Z_1} c_{\theta_Z}}{g v} X_A^f \sqrt{2 + t_\beta^2 + t_\beta^{-2}}, \\ C_{2V}^f &= c_V^f c_{\theta_Z} - \frac{c_W m_{Z_1} s_{\theta_Z}}{g v} X_V^f \sqrt{2 + t_\beta^2 + t_\beta^{-2}}, \\ C_{2A}^f &= c_A^f c_{\theta_Z} - \frac{c_W m_{Z_1} s_{\theta_Z}}{g v} X_A^f \sqrt{2 + t_\beta^2 + t_\beta^{-2}}, \end{aligned} \quad (34)$$

with $c_V^f = T_f^3 - 2s_W^2 Q_f$, $c_A^f = T_f^3$ given in terms of the weak isospin T_f^3 and the electric charge Q_f of the fermion f , and $X_V^f = (0, 1/2, -1/2, 0, 1, -1, 0, 0)$ and $X_A^f = (0, 1/2, -1/2, 0, 0, 0, 0, 0)$ for $f = (\nu_e, \nu_\mu, \nu_\tau, e, \mu, \tau, u, d)$. Because only vector currents are involved in the Z' couplings to the charged leptons, $X_A^\ell = 0$. However, $X_A^{\nu_\mu, \nu_\tau}$ are nonvanishing because neutrinos are left-handed particles in the model.

III. PHENOMENOLOGY

In this section, we derive the formalisms for the processes studied in this work. These include the cross section for CE ν NS via the $Z' - Z$ mixing, the $R(D)$ and $R(D^*)$ from LQ interactions, new Higgs decay modes, lepton $g - 2$, and the effects on the oblique parameters and the W mass.

A. CE ν NS through the $Z' - Z$ mixing

In the model, elastic electron- and muon-neutrino (including antineutrino) scatterings off a nucleus arise from gauge interactions with the neutral gauge bosons Z_1 and Z_2 . Using the gauge couplings given in Eq. (33), we can write the effective Hamiltonian for neutrino scattering at the quark level as

$$\begin{aligned} \mathcal{H}_{\nu_e q \rightarrow \nu_e q} &= \sqrt{2} G_F \left(\frac{m_Z c_{\theta_Z}}{m_{Z_2}} \right)^2 [1 + \Delta^\ell(q^2)] \\ &\quad \times [\bar{\nu}_\ell \gamma^\mu P_L \nu_\ell] [\bar{q} \gamma_\mu (c_V^q - c_A^q \gamma_5) q], \end{aligned} \quad (35)$$

$$\begin{aligned} \Delta^\ell(q^2) &= \text{sign}(\theta_Z) \frac{m_{Z_1}^2}{c_{\theta_Z}^2 (q^2 + m_{Z_1}^2)} \frac{m_{Z_2}^2}{m_Z^2 t_\beta^2} \left(1 + \delta_\mu^\ell \frac{1 + t_\beta^2}{2} \right) \\ &\simeq \text{sign}(\theta_Z) \frac{m_{Z_1}^2}{q^2 + m_{Z_1}^2} \left(\frac{1}{t_\beta^2} + \frac{\delta_\mu^\ell}{2} \right), \end{aligned} \quad (36)$$

where the Kronecker delta δ_μ^ℓ indicates that only the muon neutrino or anti-muon-neutrino contributes. The second line in Eq. (36) results from the limits of $c_{\theta_Z} \simeq 1$, $m_{Z_2} \simeq m_Z$ and large t_β . We will demonstrate that due to the $h \rightarrow HH$ and $h \rightarrow Z_1 Z_1$ constraints, a large t_β is required for the

model. As a result, the electron-neutrino scattering becomes insignificant and negligible. Since the structure of the four-fermion interaction in Eq. (35) is the same as that in the SM, the new physics contribution can be obtained simply by replacing C_{SM} with $C_{\text{SM}}[1 + \Delta^\ell(q^2)]$. In contrast to the effects induced by the kinetic mixing in the conventional $U(1)_{\mu-\tau}$ model, the $g_{Z'}$ dependence has been absorbed into m_{Z_1} . Thus, the new physics effect depends only on m_{Z_1} in the large- t_β scheme. Because the LQ mass is of $\mathcal{O}(1)$ TeV, its contribution is negligible. As such, we skip the discussion related to the LQ effects.

The cross section for the elastic neutrino-nucleus scattering can be written as [13]

$$\frac{d\sigma}{dE_r} = \frac{G_F^2 m_A}{\pi} \left(1 - \frac{m_A E_r}{2E_\nu^2} - \frac{E_r}{E_\nu} \right) |Q_w^\ell(q^2)|^2, \quad (37)$$

$$Q_w^\ell(q^2) = Z g_p^\ell F_p(q^2) + N g_n^\ell F_n(q^2), \quad (38)$$

where m_A is the nucleus mass, $Z(N)$ is the proton (neutron) number of the target nucleus, E_ν is the incident neutrino energy, E_r is the nuclear recoil energy, and $q^2 \simeq 2m_A E_r$. The couplings to the proton g_p and the neutron g_n are, respectively, given by

$$\begin{aligned} g_p^\ell &= (2c_V^u + c_V^d)[1 + \Delta^\ell(q^2)], \\ g_n^\ell &= (c_V^u + 2c_V^d)[1 + \Delta^\ell(q^2)]. \end{aligned} \quad (39)$$

Since the contribution from the weak axial-vector currents is much smaller than that from the vector currents, we have ignored their effects in Eq. (37). To include the nuclear effects, we adopt the Klein-Nystrand approach [90] for $F_{p/n}(q^2)$, expressed as [13]

$$F_{\text{KN}}(q^2) = \frac{3j_1(qR_A)}{qR_A} \frac{1}{1 + q^2 a_K^2}, \quad (40)$$

where $R_A = 1.2A^{1/3}$ with A being the mass number, j_1 is the spherical Bessel function of order one, and a_K denotes the range of a short-range Yukawa potential. For a numerical estimate, we take $a_K = 0.7$ fm. The neutrinos detected in the COHERENT experiment are produced by the stopped π^+ decay via $\pi^+ \rightarrow \nu_\mu + \mu^+$ and by the subsequent μ^+ decay through $\mu^+ \rightarrow e^+ + \nu_e + \bar{\nu}_\mu$. In this study, we assume that the shapes of neutrino fluxes are the same as their energy spectra, expressed as [4,91,92]

$$\begin{aligned} \frac{d\phi_\mu(E_\nu)}{dE_\nu} &= \mathcal{N} \delta \left(E_\nu - \frac{m_\pi^2 - m_\mu^2}{2m_\pi} \right), \\ \frac{d\phi_{\bar{\mu}}(E_\nu)}{dE_\nu} &= \mathcal{N} \frac{64 E_\nu^2}{m_\mu m_\mu^2} \left(\frac{3}{4} - \frac{E_\nu}{m_\mu} \right), \\ \frac{d\phi_e(E_\nu)}{dE_\nu} &= \mathcal{N} \frac{192 E_\nu^2}{m_\mu m_\mu^2} \left(\frac{1}{2} - \frac{E_\nu}{m_\mu} \right), \end{aligned} \quad (41)$$

with \mathcal{N} being a normalization factor. Hence, the total cross section averaged over the neutrino fluxes can be obtained as

$$\langle \sigma \rangle_\phi = \sum_{\ell=e,\mu,\bar{\mu}} \int_{E_\nu^{\min}}^{E_\nu^{\max}} dE'_\nu \int_{E_r^{\min}}^{E_r^{\max}} dE_r \frac{d\sigma(\nu_\ell A \rightarrow \nu_\ell A) d\phi_\ell(E'_\nu)}{dE_r dE'_\nu}, \quad (42)$$

where $E_r^{\max,\nu_\mu} = 2E_{\nu_\mu}^2 / (m_A + 2E_{\nu_\mu})$, $E_{\nu_\mu} = (m_\pi^2 - m_\mu^2) / 2m_\pi$, $E_r^{\max,\nu_{e,\bar{\mu}}} = 2E_{\nu'}^2 / (m_A + 2E_{\nu'})$, $E_{\nu'}^{\max} = m_\mu / 2$, E_r^{\min} denotes the nuclear threshold recoil energy, and E_ν^{\min} is the minimum incident neutrino energy required to reach E_r^{\min} .

B. $R(D)$ and $R(D^*)$

The model has two different mechanisms contributing to the $b \rightarrow c\ell\nu$ process: One involves the charged Higgs boson, and the other is from the LQ. However, the effects of the charged Higgs are not significant as its couplings to quarks and leptons are suppressed by $m_{b,c,\ell} / (vt_\beta)$. We thus focus exclusively on the LQ contributions. Based on the Yukawa couplings of LQ in Eq. (32), the effective Hamiltonian for $b \rightarrow c\ell\nu$ mediated by the W gauge boson and S^\ddagger can be obtained as [80]

$$\mathcal{H}_{b \rightarrow c\ell\nu} = \frac{4G_F V_{cb}}{\sqrt{2}} \left[(\delta_\ell^\ell + C_V^\ell \delta_\tau^\ell) \bar{c} \gamma^\mu P_L b \bar{\ell} \gamma_\mu P_L \nu_\ell + C_S^\ell \bar{c} P_L b \bar{\ell} P_L \nu_\ell + C_T^\ell \bar{c} \sigma_{\mu\nu} P_L b \bar{\ell} \sigma^{\mu\nu} P_L \nu_\ell \right], \quad (43)$$

where the effective Wilson coefficients at the m_S scale are given as

$$\begin{aligned} C_V^\ell &= \frac{\sqrt{2}}{4G_F V_{cb}} \frac{y_{L3}^q y_{L2}^q V_{L\ell\tau}^\ell}{2m_S^2}, \\ C_S^\ell &= -\frac{\sqrt{2}}{4G_F V_{cb}} \frac{y_{L3}^q y_{R2}^u V_{L\ell\tau}^\ell}{2m_S^2}, \\ C_T^\ell &= \frac{\sqrt{2}}{4G_F V_{cb}} \frac{y_{L3}^q y_{R2}^u V_{L\ell\tau}^\ell}{8m_S^2}. \end{aligned} \quad (44)$$

We note that since the electron does not mix with the μ and τ leptons, the $b \rightarrow ce\nu$ process only arises from the SM contribution. In addition, because the LQ contribution to $b \rightarrow c\ell\nu$ only involves the tau neutrino, the induced $b \rightarrow c\mu\nu_\tau$ decay does not interfere with the SM contribution. The effective couplings C_S^ℓ and C_T^ℓ at the m_b scale can be obtained from the LQ mass scale via the renormalization

group (RG) equations. Following the results in Ref. [93], we obtain $C_S^\ell(m_b) \approx 1.57 C_S^\ell(m_S)$ and $C_T^\ell(m_b) = 0.86 C_T^\ell(m_S)$.

To calculate the BRs for the $\bar{B} \rightarrow (D, D^*)\ell\nu$ decays, one requires the hadronic effects for the $B \rightarrow D^{(*)}$ transitions. The parametrization of form factors for different weak currents can be found in Appendix A 1. By utilizing these form factors, the differential decay rate for the $\bar{B} \rightarrow D\ell\bar{\nu}$ process as a function of the invariant mass q^2 of $\ell\nu$ can be expressed as

$$\begin{aligned} \frac{d\Gamma_D^\ell}{dq^2} &= \frac{G_F^2 |V_{cb}|^2 \sqrt{\lambda_D}}{256\pi^3 m_B^3} \\ &\times \left(1 - \frac{m_\ell^2}{q^2} \right)^2 \left[\frac{2}{3} \left(2 + \frac{m_\ell^2}{q^2} \right) (\delta_\mu^\ell |X_+^\ell|^2 + |X_+^\ell|^2) \right. \\ &+ \frac{2m_\ell^2}{q^2} \left(\delta_\mu^\ell |X_0^\ell|^2 + \left| X_0^\ell + \frac{\sqrt{q^2}}{m_\ell} X_S^\ell \right|^2 \right) \\ &\left. + 16 \left(\frac{2}{3} \left(1 + \frac{2m_\ell^2}{q^2} \right) |X_T^\ell|^2 - \frac{m_\ell}{\sqrt{q^2}} X_T^\ell X_0^\ell \right) \right], \end{aligned} \quad (45)$$

where $X_{+,0,S,T}^\ell$ and λ_M are defined as

$$\begin{aligned} X_+^{\ell,\mu,\tau} &= \sqrt{\lambda_D} F_+(1, C_V^\mu, 1 + C_V^\tau), \\ X_0^{\ell,\mu,\tau} &= (m_B^2 - m_D^2) F_0(1, C_V^\mu, 1 + C_V^\tau), \\ X_S^\ell &= (m_B + m_D) C_S^\ell \sqrt{q^2} F_S, \\ X_T^\ell &= -\frac{\sqrt{q^2} \lambda_D}{m_B + m_D} C_T^\ell F_T, \\ \lambda_M &= m_B^4 + m_M^4 + q^4 - 2(m_B^2 m_M^2 + m_M^2 q^2 + q^2 m_B^2). \end{aligned} \quad (46)$$

The q^2 dependence of the form factors has been suppressed.

The $\bar{B} \rightarrow D^* \ell \bar{\nu}_\ell$ decay involves D^* polarizations, and the transition form factors are more complicated. Using the parametrization in Eq. (A2), the differential decay rate after summing all D^* helicities is given by:

$$\begin{aligned} \frac{d\Gamma_{D^*}^\ell}{dq^2} &= \sum_{h=L,+,-} \frac{d\Gamma_{D^*}^{\ell h}}{dq^2} = \frac{G_F^2 |V_{cb}|^2 \sqrt{\lambda_{D^*}}}{256\pi^3 m_B^3} \\ &\times \left(1 - \frac{m_\ell^2}{q^2} \right)^2 \sum_{h=L,+,-} V_{D^*}^{\ell h}(q^2), \end{aligned} \quad (47)$$

where λ_{D^*} can be found in Eq. (46), and

$$\begin{aligned} V_{D^*}^{\ell L}(q^2) &= \frac{2}{3} \left(2 + \frac{m_\ell^2}{q^2} \right) (\delta_\mu^\ell |h_0^\ell|^2 + |h_0^\ell|^2) + \frac{2}{3} \left(1 + 2\frac{m_\ell^2}{q^2} \right) |h_T^{0\ell}|^2 \\ &+ \frac{2m_\ell^2}{q^2} \lambda_{D^*} \left(\delta_\mu^\ell |X_V^e A_0|^2 + \left| X_V^e A_0 + \frac{C_S^\ell q^2 F_P}{m_\ell (m_B + m_{D^*})} \right|^2 \right) - \frac{16m_\ell}{\sqrt{q}} h_0^\ell h_T^{0\ell}, \\ V_{D^*}^{\ell \pm}(q^2) &= \frac{2q^2}{3} \left(2 + \frac{m_\ell^2}{q^2} \right) (\delta_\mu^\ell |h_\pm^\ell|^2 + |h_\pm^\ell|^2) + \frac{32q^2}{3} \left(1 + \frac{2m_\ell^2}{q^2} \right) |h_T^{\pm\ell}|^2 - 16m_\ell \sqrt{q^2} h_\pm^\ell h_T^{\pm\ell}. \end{aligned} \quad (48)$$

The quantities h_0^ℓ , $h_T^{0\ell}$, h_\pm^ℓ , and $h_T^{\pm\ell}$ are defined by

$$\begin{aligned} h_0^{e,\mu,\tau} &= \frac{X_V^{e,\mu,\tau}}{2m_{D^*}} \left((m_B^2 - m_{D^*}^2 - q^2)(m_B + m_{D^*})A_1 \right. \\ &\quad \left. - \frac{\lambda_{D^*}}{m_B + m_{D^*}}A_2 \right), \\ h_T^{0\ell} &= \frac{C_T^\ell \sqrt{q^2}}{2m_{D^*}} \left((m_B^2 + 3m_{D^*}^2 - q^2)T_2 - \frac{\lambda_{D^*}}{m_B^2 - m_{D^*}^2}T_3 \right), \\ h_\pm^{e,\mu,\tau} &= X_V^{e,\mu,\tau} \left[(m_B + m_{D^*})A_1 \mp \frac{\sqrt{\lambda_{D^*}}}{m_B + m_{D^*}}V \right], \\ h_T^{\pm\ell} &= \frac{C_T^\ell}{\sqrt{q^2}} [(m_B^2 - m_{D^*}^2)T_2 \pm \sqrt{\lambda_{D^*}}T_1], \end{aligned} \quad (49)$$

with $X_V^{e,\mu,\tau} = (1, C_V^\mu, 1 + C_V^\tau)$, respectively. Based on Eqs. (45) and (47), $R(M)$ ($M = D, D^*$) can be calculated by

$$R_M = \frac{\int_{m_\tau^2}^{q_{\max}^2} dq^2 \frac{d\Gamma_M^\tau}{dq^2}}{\int_{m_\tau^2}^{q_{\max}^2} dq^2 \frac{d\Gamma_M^\ell}{dq^2}}, \quad (50)$$

with $q_{\max}^2 = (m_B - m_M)^2$ and $\Gamma_M^\ell = (\Gamma_M^e + \Gamma_M^\mu)/2$.

C. New Higgs decays

Equation (21) shows that utilizing an additional Higgs doublet to spontaneously break the $U(1)_{\mu-\tau}$ gauge symmetry leads to a strong correlation among m_{Z_1} , $g_{Z'}$, and t_β . As a result, several processes involving the same set of parameters exhibit distinct behaviors. In the following, we discuss these interesting processes.

With focus on the scenario with $m_H < m_h/2$ and $m_{Z_1} < 200$ MeV, the new Higgs decay channels $h \rightarrow HH$ and $h \rightarrow (Z_1 Z_1, Z_1 Z_2)$ become kinematically accessible. Using the Higgs trilinear and gauge couplings given in Eqs. (16) and (22), the partial decay rates for these channels are obtained as

$$\begin{aligned} \Gamma(h \rightarrow HH) &= \frac{m_h}{32\pi} \left(\frac{\xi m_h^2}{v^2} \right) \left(1 + \frac{2m_H^2}{m_h^2} \right)^2 \sqrt{1 - \frac{4m_H^2}{m_h^2}}, \\ \text{with } \xi &= s_{\beta-\alpha}^2 (c_{\beta-\alpha} + t_\beta s_{\beta-\alpha})^2 (c_{\beta-\alpha} - t_\beta^{-1} s_{\beta-\alpha})^2, \end{aligned} \quad (51)$$

$$\begin{aligned} \Gamma(h \rightarrow Z_1 Z_1) &\simeq \frac{m_h}{32\pi} \frac{m_h^2}{v^2} \left(s_{\beta-\alpha} - \frac{t_\beta^2 - 1}{t_\beta} c_{\beta-\alpha} \right)^2, \\ \Gamma(h \rightarrow Z_1 Z_2) &\simeq \frac{m_h}{16\pi} \left(\frac{gm_h}{2c_W m_{Z_2}} c_{\beta-\alpha} \right)^2 \left(1 - \frac{m_{Z_2}^2}{m_h^2} \right)^3. \end{aligned} \quad (52)$$

In the decoupling limit when $s_{\beta-\alpha} \rightarrow 1$, as required by the current Higgs signal strength measurements, the processes $h \rightarrow (HH, Z_1 Z_1)$ can in principle have large decay rates. Hence, the observed Higgs width Γ_h strongly constrains the

values of t_β and $c_{\beta-\alpha}$. Therefore, from Eq. (51), the condition of $c_{\beta-\alpha} \sim s_{\beta-\alpha}/t_\beta \ll 1$ has to be satisfied; i.e., a large t_β scheme is demanded by data in the model. Interestingly, when we use a large t_β value, the same condition can be used to suppress the partial decay width of $h \rightarrow Z_1 Z_1$. Moreover, since $h \rightarrow Z_1 Z_2$ does not depend on the t_β parameter, we can use the limit of $\Gamma(h \rightarrow Z_1 Z_2)$ as an independent constraint on $c_{\beta-\alpha}$. Although our analysis does not focus on the search for collider signals, the percent-level BR for $h \rightarrow Z_1 Z_2$ with invisible Z_1 decay could be an interesting channel for detecting the new physics. We note that $c_{\beta-\alpha} \sim 0.1$ is still permissible when considering the constraints from the current measurements of Higgs decays. We will see later that the BRs of new Higgs decay modes can reach the percent level with $c_{\beta-\alpha} \sim 0.05$.

In addition to the flavor-conserving Higgs Yukawa couplings, which are suppressed by m_ℓ/v according to Eq. (25), there is a tree-level LFV Higgs coupling, i.e., $h\bar{\mu}_L\tau_R$, where the strength of this LFV coupling is primarily determined by $\chi_{\mu\tau} c_{\beta-\alpha} \sqrt{m_\mu m_\tau}/(s_{2\beta} v)$. The partial decay rate for $h \rightarrow \mu\tau$ can thus be written as

$$\begin{aligned} \Gamma(h \rightarrow \mu\tau) &= \frac{m_h}{16\pi} |c_{\beta-\alpha} \zeta_{\mu\tau}|^2, \\ \text{with } \zeta_{\mu\tau} &= \frac{\sqrt{m_\mu m_\tau}}{v} \chi_{\mu\tau} \sqrt{2 + t_\beta^2 + t_\beta^{-2}}. \end{aligned} \quad (53)$$

When $c_{\beta-\alpha}$ and t_β are determined from the processes $h \rightarrow HH/Z_1 Z_2$, the $h \rightarrow \mu\tau$ decay rate then depends only on $\chi_{\mu\tau}$.

From Eq. (33), it can be seen that the tree-level lepton FCNC arises not only from the Higgs couplings but also from the Z_i couplings. For a light Z_1 gauge boson, the $\tau \rightarrow \mu Z_1$ decay can be induced at the tree level, and the BR can be obtained as

$$\text{BR}(\tau \rightarrow \mu Z_1) \simeq \frac{m_\tau (g_{Z'} q_X s_{2\theta_L} c_{\theta_Z})^2}{32\pi\Gamma_\tau} \left(1 + \frac{m_\tau^2}{m_{Z_1}^2} \right), \quad (54)$$

where we have dropped the $m_{\mu,Z_1}/m_\tau$ factors because $m_{\mu,Z_1} \ll m_\tau$. The $1/m_{Z_1}^2$ factor in the parentheses from the contribution of the longitudinal component of Z_1 will largely enhance the BR as m_{Z_1} is taken at the sub-GeV level. Since the BR of this decay is mainly determined by $g_{Z'}$, m_{Z_1} , and s_{θ_L} , we can use $\tau \rightarrow \mu Z_1$ to constrain the θ_L parameter when $g_{Z'}$ and m_{Z_1} are fixed by other processes.

D. Lepton ($g-2$)'s

Our model makes additional contributions to the lepton ($g-2$)'s through the mediations of Z_1 , H , and LQ at the one-loop level. One can neglect the contribution from LQ as it is suppressed by m_μ^2/m_Σ^2 . Based on the gauge couplings given in Eq. (33), although the LFV coupling $\mu\tau Z_1$ can

contribute to the muon and tau ($g-2$)'s, its effect is negligible as the coupling is proportional to $g_{Z'}s_{\theta_L}$, where $g_{Z'}$ is of $\mathcal{O}(10^{-4})$, and s_{θ_L} is highly constrained by the $\tau \rightarrow \mu Z_1$ decay, as argued at the end of last subsection. On the contrary, the contribution from the light H is through the LFV coupling $\mu\tau H$. From Eq. (25), it can be seen that although this coupling is suppressed by a factor of m_ℓ/v , the factor $1/c_\beta$ can enhance the lepton ($g-2$)'s in the regime of large t_β and small m_H .

The explicit expressions of the Z_1 and H contributions to the lepton ($g-2$)'s are, respectively, given by:

$$\Delta a_{\ell'}^{Z_1} = \frac{g^2}{32\pi^2 c_W^2} (C_{1V}^{\ell'} + C_{1A}^{\ell'}) \int_0^1 dx \frac{2m_\ell^2 x^2 (1-x)}{m_{Z_1}^2 (1-x) + m_\ell^2 x^2},$$

$$- \frac{g^2}{32\pi^2 c_W^2} C_{1A}^{\ell'} \int_0^1 dx \frac{8m_\ell^2 x(1-x)}{m_{Z_1}^2 (1-x) + m_\ell^2 x^2}, \quad (55)$$

$$\Delta a_{\ell'}^H = \frac{m_{\ell'}^2}{8\pi^2 m_H^2} |s_{\beta-\alpha} \zeta_{\mu\tau}|^2, \quad (56)$$

with $\ell = (e, \mu, \tau)$ and $\ell' = (\mu, \tau)$. Although the couplings of Z_2 , excluding the SM part, can contribute to the lepton ($g-2$)'s, the suppression factors of $(s_{\theta_Z}, g_{Z'})m_\ell^2/m_{Z_2}^2$ make the effects negligible. We, therefore, disregard the new physics contribution from Z_2 .

E. Oblique parameters and the W mass

An important set of precision measurements for constraining new physics comprises the oblique parameters denoted by S , T , and U . These quantities are related to the loop-induced vacuum polarizations of vector gauge bosons, and their detailed definitions can be found in Refs. [94,95]. In our model, in addition to the SM-like Higgs doublet H_2 , the oblique parameters receive effects from the extra $SU(2)$ Higgs doublet H_1 and the new gauge coupling to Z' . Since we will focus on $g_{Z'} \sim \mathcal{O}(10^{-4})$, we ignore the Z' contribution and take $m_{Z_2} \simeq m_Z$ in the analysis. However, a distinctive difference is that the pseudoscalar in the conventional 2HDM becomes the longitudinal component of Z' . Thus, the main contributions running in the loops to the oblique parameters are from H^\pm , h , and H .

To calculate the S , T , and U parameters in the model, we use the results obtained in Ref. [96], where the resulting oblique parameters are suitable for the multi-Higgs-doublet models and even for the models with new singlet charged scalars. Except for the absence of pseudoscalar contributions, the effects from H^\pm , h , and H are similar to the conventional 2HDM. The detailed expressions for the S , T , and U parameters as functions of the scalar masses and couplings are given in Appendix B.

Using the obtained oblique parameters, the W mass under the influence of new radiative corrections can be expressed as [95,97,98]

$$m_W \equiv m_W^{\text{SM}} \delta_O = m_W^{\text{SM}} \left[1 + \frac{\alpha_{\text{em}}}{c_W^2 - s_W^2} \times \left(c_W^2 T - \frac{S}{2} + \frac{c_W^2 - s_W^2}{4s_W^2} U \right) \right]^{1/2}, \quad (57)$$

where m_W^{SM} denotes the W mass in the SM, and its relationship with m_Z is defined to be the same as that in the SM; i.e., $m_W^{\text{SM}} = m_Z c_W$. It is worth mentioning that the tree-level $Z' - Z$ mixing can affect the oblique parameters and modify the relation between m_W^{SM} and m_Z [98]. However, since the mixing angle θ_Z in the model is of $\mathcal{O}(10^{-5})$ in our study, the effects can be safely ignored.

IV. NUMERICAL ANALYSIS AND DISCUSSIONS

Before conducting a numerical analysis of the physical processes studied in this work, we should first find the viable ranges of new physics parameters in the $U(1)_{\mu-\tau}$ -extended model. For example, as alluded to before, the most influential parameter for the CE ν NS is m_{Z_1} , and its cross section can be potentially enhanced by a larger value of m_{Z_1} . The magnitude of m_{Z_1} , on the other hand, is proportional to $g_{Z'}$ whose value can be constrained by, e.g., the observed muon $g-2$. In the following, we start by setting bounds on the parameter space and then make predictions for the CE ν NS cross section, $R(D^{(*)})$, and the oblique parameters and W boson mass. We will also study the decays of the Z_1 and H bosons in the model.

A. Constraints of parameters

The free parameters considered in this study are m_H , m_{Z_1} , m_S , $g_{Z'}$, $\chi_{\mu\tau}$, $c_{\beta-\alpha}$, and t_β , where $\chi_{\mu\tau}$ parametrizes the $\mu - \tau$ mixing effect through $s_{\theta_L} \simeq \chi_{\mu\tau} \sqrt{m_\mu/m_\tau}$, and the $Z' - Z$ mixing is determined by m_{Z_1} and t_β . Based on the constraints from the neutrino trident process [99], measured by CCFR [100], and the 4μ final states in the BABAR experiment [101], we can conservatively take the bounds of $g_{Z'} q_X \lesssim 1.3 \times 10^{-3}$ and $m_{Z_1} < 200$ MeV. According to Eq. (55), the Z_1 boson makes an important contribution to the muon $g-2$. Therefore, we show in Fig. 1 the CCFR bound [99] and the $\pm 3\sigma$ contours (blue dot-dashed curves) of the measured muon $g-2$ in the m_{Z_1} - $g_{Z'} q_X$ plane, where the shaded region above the red dashed curve is ruled out by the CCFR experiment. Although $\Delta a_\mu^{Z_1}$ depends on t_β via the $Z' - Z$ mixing, its effect is negligibly small because $s_\theta \sim \mathcal{O}(10^{-5})$ in the considered range of m_{Z_1} . As a result, the electron $g-2$ mediated by Z_1 and induced through $Z' - Z$ mixing is estimated to be $\Delta a_e^{Z_1} \approx -1.4 \times 10^{-16}$, completely negligible. We will show later that due to the small lepton flavor mixing, as constrained by other processes, the effect mediated by H for the lepton $g-2$ is also highly suppressed. In the model, m_{Z_1} and $g_{Z'} q_X$ are

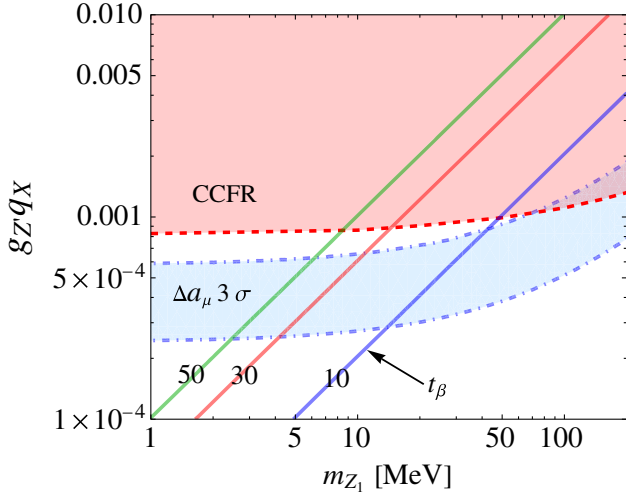


FIG. 1. Parameter space preferred by the muon $g - 2$ (shaded region bounded by blue dot-dashed curves) and ruled out by the CCFR experiment (shaded region above the red dashed curve). The solid lines represent the contours for t_β .

not independent parameters and are related by $m_{Z_1} = 2vt_\beta g_{Z'q_X} / (1 + t_\beta^2)$. In Fig. 1, we also show contours of t_β using solid lines. The large t_β scheme, as required to restrict the $h \rightarrow HH$ and $h \rightarrow Z_1 Z_1$ rates, to be discussed in more detail below, further narrows down the preferred m_{Z_1} range.

The SM prediction for the Higgs boson width is $\Gamma_h^{\text{SM}} \approx 4.1$ MeV [102], while the current measurement gives $\Gamma_h^{\text{exp}} = 3.2^{+2.8}_{-2.2}$ MeV [103]. As an illustrated example, we assume that each new Higgs decay channel in the model contributes less than 5% of Γ_h^{SM} , i.e., $\Gamma_h^{\text{NP}} \leq 0.20$ MeV. This assumption is consistent with the current upper limit on the Higgs invisible decays, $\text{BR}(h \rightarrow \text{invisible}) < 0.19$ [103]. To fit the observed Higgs signal strengths, the Higgs couplings to the fermions and the W^\pm and Z gauge bosons should have $s_{\beta-\alpha} \approx 1$.

We now use $\Gamma(h \rightarrow HH)$ to bound $c_{\beta-\alpha}$ and t_β . Since the $h \rightarrow HH$ process depends on m_H , we show the upper bound on ξ , defined in Eq. (51), for some benchmarks of m_H :

$$\xi \lesssim \frac{10^{-3} \Gamma(h \rightarrow HH)}{0.20 \text{ MeV}} \times \begin{cases} 0.59 & m_H = 30 \text{ GeV}, \\ 0.61 & m_H = 50 \text{ GeV}, \\ 1.07 & m_H = 60 \text{ GeV}. \end{cases} \quad (58)$$

To illustrate the dependence of ξ on $c_{\beta-\alpha}$ and t_β , we show in Fig. 2 the contour plot of ξ in the t_β - $c_{\beta-\alpha}$ plane, where we have fixed $\xi = 0.61 \times 10^{-3}$ and $\Gamma(h \rightarrow HH) = 0.20$ MeV. It is found that there are two slightly separated contours, which are insensitive to the chosen value of ξ and indicate that $c_{\beta-\alpha}$ decreases as t_β increases. With the choice of $t_\beta = 25$, $m_H = 50$ GeV, and $\xi = 0.61 \times 10^{-3}$, we obtain

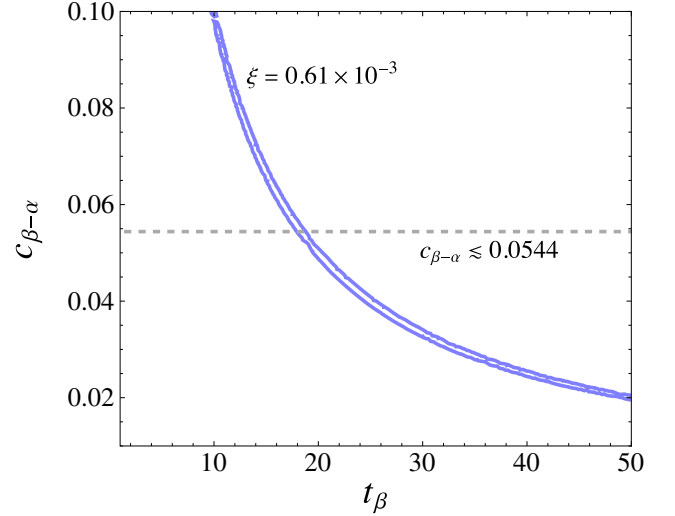


FIG. 2. Contours of ξ (blue solid curves) in the t_β - $c_{\beta-\alpha}$ plane, assuming $\xi = 0.61 \times 10^{-3}$ and $\Gamma(h \rightarrow HH) = 0.20$ MeV. The dashed line denotes the upper bound on $c_{\beta-\alpha}$ from $\Gamma(h \rightarrow Z_1 Z_2) \leq 0.20$ MeV.

$c_{\beta-\alpha} \approx 4.095\%$ and $s_{\beta-\alpha} \approx 99.92\%$. The values in turn determine that $\Gamma(h \rightarrow Z_1 Z_1) \approx 0.17$ MeV and $\Gamma(h \rightarrow Z_1 Z_2) \approx 0.11$ MeV.

In the large t_β scheme, $\Gamma(h \rightarrow Z_1 Z_2)$ only depends on $c_{\beta-\alpha}$. With $m_h = 125$ GeV and $m_{Z_2} = 91.187$ GeV, the limit of $c_{\beta-\alpha}$ can be determined as

$$c_{\beta-\alpha} \lesssim 0.0544 \left(\frac{\Gamma(h \rightarrow Z_1 Z_2)}{0.20 \text{ MeV}} \right)^{1/2}. \quad (59)$$

The assumption of $\Gamma(h \rightarrow Z_1 Z_2) \leq 0.20$ MeV then translates into the dashed line in Fig. 2. According to the result in Eq. (21), we can estimate the $Z' - Z$ mixing angle to have

$$|s_{\theta_Z}| \approx 1.08 \times 10^{-5} \left(\frac{20}{t_\beta} \right) \left(\frac{m_{Z_1}}{20 \text{ MeV}} \right). \quad (60)$$

Clearly, s_{θ_Z} can be larger than the loop-induced kinetic mixing between Z' and γ , characterized by the mixing parameter [28,104]:

$$\epsilon = \frac{g_{Z'e}}{6\pi^2} \ln \frac{m_\tau}{m_\mu} \approx 8.68 \times 10^{-6} \left(\frac{g_{Z'}}{6 \times 10^{-4}} \right). \quad (61)$$

Consequently, we concentrate on the contributions from the $Z' - Z$ mixing in this study.

The $\chi_{\mu\tau}$ parameter contributes to $h \rightarrow \mu\tau$, $\tau \rightarrow \mu Z_1$, and Δa_μ^H . Since the $\tau \rightarrow \mu Z_1$ process is strongly enhanced by the factor of $m_\tau^2/m_{Z_1}^2$, its measurement will put a strict constraint on $\chi_{\mu\tau}$. To bound the $\chi_{\mu\tau}$ parameter using available data, we can use the upper limit of the process

$\tau \rightarrow \mu + \text{light boson}$ as an estimate, where the current data give $\text{BR}(\tau \rightarrow \mu + \text{light boson}) < 5 \times 10^{-3}$ [103,105]. With $c_{\theta_L} \approx c_{\theta_Z} \approx 1$ and the result in Eq. (54), we obtain an upper bound on $\chi_{\mu\tau}$ as

$$\chi_{\mu\tau} < 1.82 \times 10^{-5} \left(\frac{25}{t_\beta} \right). \quad (62)$$

The resulting $\text{BR}(h \rightarrow \mu\tau)$ and Δa_μ^H are then less than $\mathcal{O}(10^{-11})$ and $\mathcal{O}(10^{-16})$, respectively.

The primary purpose of introducing the scalar LQ, S_3^\pm , in the model is to address the $R(D^{(*)})$ anomalies. Along with the mass of LQ, the related parameters are $y_{L3,L2}^q$, y_{R2}^u , and $V_{L\ell\tau}^\ell$. Due to the $\tau \rightarrow \mu Z_1$ constraint, the lepton flavor mixing matrix can be approximated as $V_L^\ell \approx 1$, allowing us to ignore its contribution to the muon mode. Consequently, the LQ only couples to the third-generation leptons. According to Eq. (32), unlike the independent couplings to the different up-type quarks, the LQ couplings to the different down-type quarks are related by the CKM matrix and can be written as

$$\begin{aligned} (V_{\text{CKM}}^T \mathbf{y}_L^q)_d &\approx \frac{10}{3} \lambda^4 y_{L3}^q - \lambda y_{L2}^q + y_{L1}^q, \\ (V_{\text{CKM}}^T \mathbf{y}_L^q)_s &\approx -\frac{4}{5} \lambda^2 y_{L3}^q + y_{L2}^q + \lambda y_{L1}^q, \\ (V_{\text{CKM}}^T \mathbf{y}_L^q)_b &\approx y_{L3}^q, \end{aligned} \quad (63)$$

where $\lambda \approx 0.2257$ is a Wolfenstein parameter, and $V_{ub} \ll V_{cb} \ll V_{tb} \approx V_{cs} \approx V_{ud} \approx 1$ has been applied. To suppress the LQ couplings to the first- and second-generation quarks so as to satisfy constraints from low-energy physics, such as $P - \bar{P}$ mixing and $q_i \rightarrow q_j \bar{f}' f'$, where P and f' are, respectively, possible neutral mesons and leptons, we require the Yukawa couplings to have the hierarchy

$$y_{L3}^q \sim \mathcal{O}(1), \quad y_{L2}^q \sim \mathcal{O}(\lambda^2), \quad y_{L1}^q \sim \mathcal{O}(\lambda^3). \quad (64)$$

If cancellations are allowed in the terms of $(V_{\text{CKM}}^T \mathbf{y}_L^q)_{d,s}$, small LQ couplings to the first two generations of down-type quarks can be easily achieved in the model. Although $D - \bar{D}$ mixing can constrain $y_{R2}^u y_{R1}^u$, we can take a small y_{R1}^u to avoid this constraint on $|y_{R2}^u|$, for which we need $y_{R2}^u \sim \mathcal{O}(0.5)$ to enhance $R(D^{(*)})$.

In this model, the LQ couplings to the third-generation quarks are dominant. Both CMS [106] and ATLAS [107] have searched for the scalar LQ with an electric charge of $e/3$ using the $\tau\tau$ and $b\nu$ production channels. ATLAS has placed a stronger upper bound on the LQ mass when $\text{BR}(S^{-1/3} \rightarrow \tau\tau) = 1/2$, obtaining $m_S \geq 1.22$ TeV. If we set $y_{R3}^u = 0$, the ATLAS measurement can be directly applied to our model, and $\tau\tau$ and $b\nu_\tau$ thus become the

dominant decays of the LQ. To be more conservative, we use $m_S = 1.5$ TeV in our numerical calculations.

B. Phenomenological analysis

Here, we present the numerical results of the observables discussed in Sec. III and highlight their features while taking into account the constrained parameter space obtained in Sec. IVA.

I. Cross sections of CE ν NS on Ar and CsI targets

Since the targets of the measured CE ν NS in the COHERENT experiment are Ar and CsI, we focus on both targets in the following numerical analysis. Because CsI is a compound of cesium and iodide, the fraction of each nucleus contributing to the cross section is defined by $f_i = A_i/(A_{\text{Cs}} + A_{\text{Ar}})$ [108]. Based on COHERENT's best-fit results for $\langle \sigma \rangle_e$ and $\langle \sigma \rangle_{\mu+\bar{\mu}}$ [3], where the resulting $\langle \sigma \rangle_{\mu+\bar{\mu}}$ is noticeably smaller than the SM prediction, we choose to present the numerical results with $\text{sign}(\theta_Z) = -1$.

To calculate the cross section of CE ν NS for Ar and CsI, the quantities involved in Eq. (42) are taken as follows: The weak mixing angle is $s_W^2 = 0.23112$, the number of the protons and neutrons in ^{40}Ar , ^{127}I , and ^{133}Cs are set to be $(Z, N)_{\text{Ar}} = (18, 22)$, $(Z, N)_{\text{I}} = (53, 74)$, and $(Z, N)_{\text{Cs}} = (55, 75)$, respectively, and the masses of the nuclei are $m_{\text{Ar}} = 37.20$ GeV, $m_{\text{I}} = 118.24$ GeV, and $m_{\text{Cs}} = 123.86$ GeV. The energy of the prompt ν_μ is determined from the π^+ decay at rest. With $m_\mu = 105.65$ MeV and $m_\pi = 139.57$ MeV, we obtain $E_{\nu_\mu} \simeq 29.80$ MeV. By neglecting the electron mass, the maximum energy of ν_e and $\bar{\nu}_\mu$ from the μ^+ decay is $E_{\nu_e, \bar{\nu}_\mu}^{\text{max}} = m_\mu/2 \simeq 52.8$ MeV.

As mentioned in the introduction, the difficulty in measuring the CE ν NS is due to the small nuclear recoil energy (RE). We can estimate the maximum RE of the nuclear targets, argon, iodine, and cesium, by incident ν_μ with the energy of 29.80 MeV as $E_r^{\text{max}, \nu_\mu} = (47.66, 15.01, 14.33)$ keV, respectively. The maximum RE of (Ar, I, Cs) from $\bar{\nu}_\mu$ or ν_e with the maximum incident energy of 52.8 MeV is given by $E_r^{\text{max}, \bar{\nu}_\mu(\nu_e)} = (149.46, 47.11, 44.98)$ keV. The nuclear threshold RE in the COHERENT experiment for (Ar, CsI) is (20, 6.5) keV [109]. Using $E_\nu \approx \sqrt{m_T E_r}/2$, the minimum neutrino energy of producing the threshold RE for Ar and CsI can be estimated to be $E_\nu^{\text{min}} \sim 19$ MeV. If we apply this E_ν^{min} to Eq. (42), it is found that the total cross section of CE ν NS will be reduced by $\sim 2.4\%$, which is the same as the uncertainty from the nuclear form factor. Due to the fact that $E_{\nu_\mu} \simeq 29.80$ MeV, the kinematic cut of $E_\nu^{\text{min}} \sim 19$ MeV does not influence the ν_μ scattering. Additionally, according to neutrino fluxes shown in Eq. (41), $E_\nu \lesssim 19$ MeV locates at the front tail of the ν_e and $\bar{\nu}_\mu$ fluxes, where the

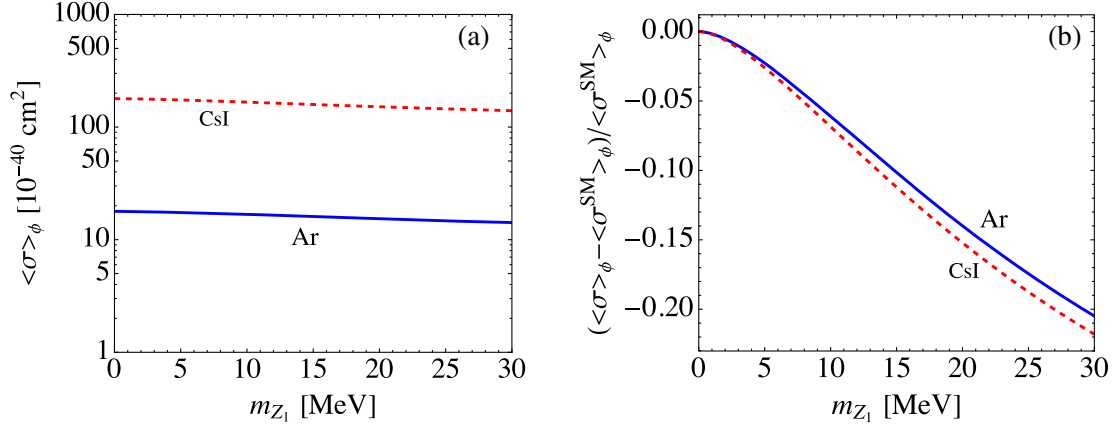


FIG. 3. (a) Cross section averaged by neutrino fluxes for Ar and CsI targets as a function of m_{Z_1} , where the points for $m_{Z_1} = 0$ correspond to the SM results. (b) Fractional deviation on the total cross section $\langle \sigma \rangle_\phi$ from its SM value as a function of m_{Z_1} . In both plots, the solid and dashed curves represent the results for Ar and CsI targets, respectively.

contributions from this region are much smaller than those from 19 to 52.80 MeV. Since our purpose is to demonstrate the sensitivity to the new physics effects, for simplicity, we do not consider the kinematic cut based on the experimental conditions. The detailed event analysis based on the experimental setup can be found in Ref. [25].

Using Eq. (42), we show the total cross section of CE ν NS for Ar (solid) and CsI (dashed) as a function of m_{Z_1} in Fig. 3(a). We estimate the SM results for Ar and CsI to be $18.2 \times 10^{-40} \text{ cm}^2$ and $183.12 \times 10^{-40} \text{ cm}^2$, respectively. Since the cross section is plotted in the logarithmic scale, the sensitivity in m_{Z_1} is not obvious. To illustrate the new physics effects, we show the deviation from the SM result, defined by $(\langle \sigma^{\text{NP+SM}} \rangle_\phi - \langle \sigma^{\text{SM}} \rangle_\phi) / \langle \sigma^{\text{SM}} \rangle_\phi$, in Fig. 3(b). It can be seen that the influence of new physics can exceed 10% when $m_{Z_1} \gtrsim 12$ MeV, with a slightly larger influence on CsI than on Ar.

In addition to the total cross section of CE ν NS, the cross section at specific incident neutrino energy E_ν serves as another useful physical observable for probing the new physics effects. For clarity, we define the averaged total cross section as a function of E_ν as follows:

$$\langle \Sigma \rangle = \frac{1}{\Phi(E_\nu)} \sum_{\ell=e,\mu,\bar{\mu}} \int_{E_r^{\min}}^{E_r^{\max}} dE_r \frac{d\sigma(\nu_\ell A \rightarrow \nu_\ell A)}{dE_r} \frac{d\phi_\ell(E_\nu)}{dE_\nu},$$

$$\Phi(E_\nu) = \sum_{\ell=e,\mu,\bar{\mu}} \frac{d\phi_\ell(E_\nu)}{dE_\nu}. \quad (65)$$

In Fig. 4(a), we show $\langle \Sigma \rangle$ as a function of E_ν in the SM for the targets of Ar, I, and Cs by the solid, dot-dashed, and dashed curves, respectively. To demonstrate the sensitivity of $\langle \Sigma \rangle$ to the new physics effects, we present the results for Ar and CsI in Figs. 4(b) and 4(c), respectively, where the

solid, dot-dashed, and dashed curves denote cases with $m_{Z_1} = (0, 10, 30)$ MeV. It can be seen that the deviation from the SM increases with m_{Z_1} . To illustrate the sensitivity of $\langle \Sigma \rangle$ on the Z' mass, we exhibit $\delta\langle \Sigma \rangle = (\langle \Sigma^{\text{NP+SM}} \rangle - \langle \Sigma^{\text{SM}} \rangle) / \langle \Sigma^{\text{SM}} \rangle$ in Fig. 4(d) for Ar and CsI, where the dot-dashed and dashed curves are for $m_{Z_1} = 10$ and 30 MeV. From the results, we find that the sensitivity level $|\delta\langle \Sigma \rangle|$ first decreases with E_ν and then turns to increase with E_ν at some higher E_ν , e.g., at $E_\nu \sim (41, 36)$ MeV for $m_{Z_1} = (10, 30)$ MeV. Hence, the deviation from the SM result can reach $\sim 11\%$ (22%) at $E_\nu = 15$ MeV and $\sim 7\%$ (25%) at $E_\nu = 50$ MeV for $m_{Z_1} = 10$ (30) MeV.

As stated in the introduction, a light Z' gauge boson can be realized by a variety of local $U(1)$ gauge symmetries. The gauged $U(1)$ symmetries can be classified as $U(1)_{X_q - \sum_\ell c_\ell X_\ell}$, where $X_{q,\ell}$ denote the $U(1)$ charges of quark and lepton, respectively. Since the experiments from the searches of visible dark photons place strict constraints on $g_{Z'}$ and $m_{Z'}$, not all $U(1)$ models are of interest in the study. To illustrate the contributions from different gauged $U(1)$ symmetries to CE ν NS, we consider the potential models, including universal, $B - L$, $B - L_e - 2L_\mu$, and $L_\mu - L_\tau$ with kinetic mixing, from the model listed in Ref. [25], where the charge assignments of the selected $U(1)$'s are given in Table II. Using the central value of data along with 1σ errors as the upper bound for CE ν NS, the flux-averaged cross section $\langle \sigma \rangle_\phi$ for the selected $U(1)$ models as a function of $g_{Z'}$ and $m_{Z'}$ is shown in Fig. 5, where the solid, long dashed, dotted, dashed, and dot-dashed curves represent the results from our model, universal, $B - L$, $B - L_e - 2L_\mu$, and $L_\mu - L_\tau$ with kinetic mixing, respectively. It can be seen that in the mass region of $10 \leq m_{Z'} \leq 100$ MeV, our model can fit better the constraint from CCFR and the observed muon $g - 2$.

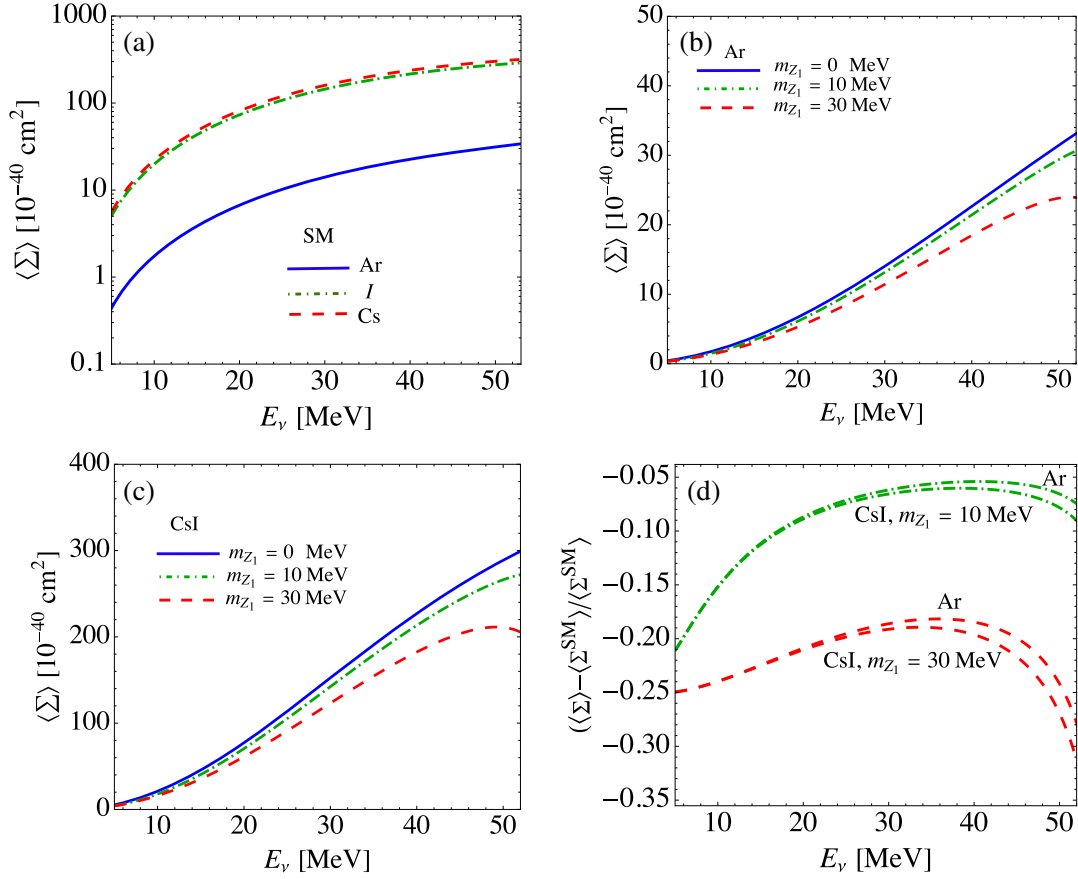


FIG. 4. (a) $\langle \Sigma \rangle$ as a function of E_ν for Ar (solid), I (dot dashed), and Cs (dashed) in the SM. $\langle \Sigma \rangle$ for (b) Ar and (c) CsI with $m_{Z_1} = 0$ MeV (solid), 10 MeV (dot dashed), and 30 MeV (dashed). (d) Sensitivity of $\langle \Sigma \rangle$ on the Z' boson for Ar and CsI with $m_{Z_1} = 10$ MeV (dot dashed) and 30 MeV (dashed).

2. $R(D)$ and $R(D^*)$ mediated by LQ

The calculations of $R(D)$ and $R(D^*)$ depend on the form factors of the $B \rightarrow (D, D^*)$ transitions. In this study, we use the form factors given in Ref. [59], obtained using the heavy quark effective theory (HQET). With the input values of $m_{B^+} = 5.28$ GeV, $m_{D^0} = 1.864$ GeV, $m_{D^{*0}} = 2.007$ GeV, $\tau_{B^+} = 2.450 \times 10^{12}$ GeV $^{-1}$, and $V_{ub} = 0.0395$, the BRs for $B^+ \rightarrow (D^0, D^{*0})\ell\nu$ are found to be consistent with current experimental data, as shown in Table III. Using the formulas presented in Sec. III B, we obtain for the SM that

$$R^{\text{SM}}(D) \approx 0.297, \quad R^{\text{SM}}(D^*) \approx 0.258. \quad (66)$$

The values are within 1σ errors of those obtained in Ref. [59] and are consistent with the results given in Refs. [56–63].

The parameters involved in the $b \rightarrow c\tau\nu$ transition mediated by the LQ appear in the combinations of $y_{L3}^q y_{L2}^q / m_S^2$ and $y_{L3}^q y_{R2}^u / m_S^2$. For the numerical analysis, we fix $m_S = 1.5$ TeV. From Eq. (63), we see that $y_{L2}^q \sim \mathcal{O}(\lambda^2) \ll y_{L3}^q$, indicating that the dominant effect

on $R(D)$ and $R(D^*)$ comes from the combination $y_{L3}^q y_{R2}^u$. To simplify the analysis, we take the assumption that $y_{L2}^q = 0$, in which case $R(D^*)$ is found to deviate from that with $y_{L2}^q = 0.04$ by only $\sim 2\%$. We present the contours of $R(D)$ and $R(D^*)$ in the y_{L3}^q - y_{R2}^u plane in the left plot of Fig. 6, with the shaded areas (light green and gray, respectively) covering the 2σ ranges of their world averages. It is seen that the low boundaries of $R(D)$ and $R(D^*)$ match exactly, while the upper boundary for $R(D) = 0.414$ is close to the contour of $R(D^*) = 0.297$. This illustrates

TABLE II. Charge assignments of the selected new $U(1)$ gauged models [25].

Model	Universal	$B - L$	$B - 3L_\mu$	$B - L_e - 2L_\mu$	$L_{\mu-\tau}$
X_u	1	1/3	1/3	1/3	0
X_d	1	1/3	1/3	1/3	0
X_e	1	-1	0	-1	0
X_μ	1	-1	-3	-2	1
X_τ	1	-1	0	0	-1

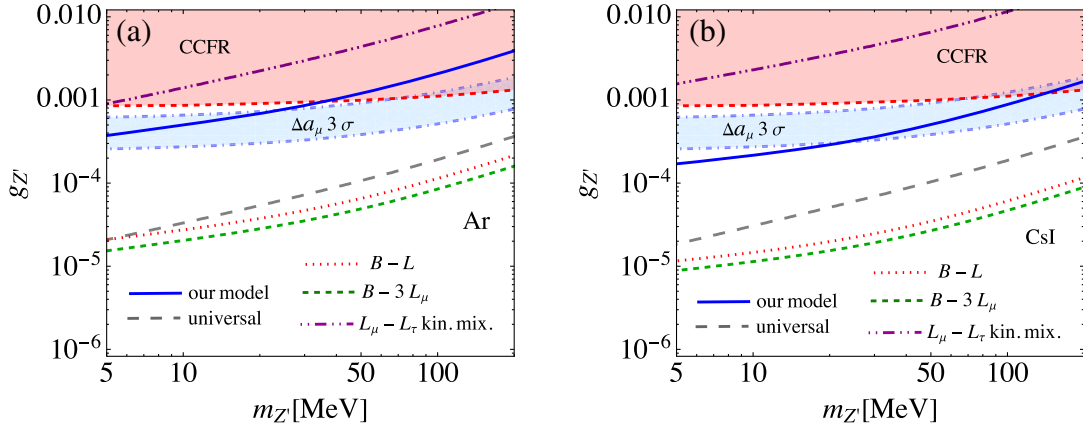


FIG. 5. Selected $U(1)$ gauged models contributing to the flux-averaged cross section $\langle\sigma\rangle_\phi$ as functions of $g_{Z'}$ and $m_{Z'}$ for the (a) Ar and (b) CsI targets, where we have taken the upper bounds of $\langle\sigma\rangle_\phi = (29, 200) \times 10^{-40}$ cm 2 for Ar and CsI, respectively.

that an accurate measurement of $R(D)$ can indirectly constrain the value of $R(D^*)$ and vice versa. The right plot of Fig. 6 shows the dependence of $R(D^*)$ on the product $y_{L3}^q y_{R2}^u$. To explain the $R(D)$ and $R(D^*)$ anomalies, we need $-1 < y_{L3}^q y_{R2}^u < 0$ for $m_{LQ} = 1.5$ TeV. It is observed that $R(D)$ is more sensitive to the S^\ddagger contribution.

In addition to the ratio of the BR for $\tau\nu$ to that for $\ell\nu$, other physical observables may be sensitive to the new physics, such as the forward-backward asymmetry of the charged lepton, τ polarization [73,75], and q^2 -dependent differential decay rates. The BR is sensitive to the CKM matrix elements and the form factors of the $B \rightarrow (D, D^*)$ transitions. To eliminate these factors, we propose the ratio of the q^2 -dependent differential decay rates, defined to be

$$R_M(q^2) = \frac{d\Gamma_M^\tau/dq^2}{d\Gamma_M^{\ell'}/dq^2} H(q^2 - m_\tau^2), \quad (67)$$

where $H(x)$ is the Heaviside step function, and $d\Gamma_M^{\ell'}/dq^2$ is the average of the electron and muon modes. Because the threshold invariant mass squared of $\tau\nu$ in the $B \rightarrow M\tau\nu$ decay is $q^2 = m_\tau^2$, we thus require that the denominator $d\Gamma_M^{\ell'}/dq^2$ also starts from the same invariant mass squared. To appreciate the benefit of considering the observable defined in Eq. (67), we first show the q^2 -dependent BRs for $B^- \rightarrow (D^0, D^{0*})\ell''\nu$ ($\ell'' = \ell', \tau$) in the SM in Figs. 7(a) and 7(b), respectively. Plot (a) shows that when

$q^2 \gtrsim 8$ GeV 2 , the decay $B^- \rightarrow D^0\tau\nu$ becomes larger than the light lepton mode, and it is expected that $R_D(q^2) > 1$ in this region. D^* is a vector meson and has longitudinal (P_L) and transverse (P_T) components. To exhibit their contributions, we separately show P_L and P_T in Fig. 7(b). The results indicate that P_T becomes larger than P_L at somewhat large q^2 regions in both light lepton and τ modes. In contrast to the $B^- \rightarrow D^0\ell''\nu$ decay, $d\Gamma_{D^*}^{\ell'}/dq^2$ is always larger than $d\Gamma_{D^*}^\tau/dq^2$ in the allowed kinematic region; thus, it is expected that $R_{D^*}(q^2) < 1$.

The q^2 dependence of $R_D(q^2)$ and $R_{D^*}(q^2)$ in the SM is shown in Figs. 7(c) and 7(d), respectively, using the solid curves. It is confirmed that $R_D(q^2) \gtrsim 1$ at $q^2 \gtrsim 8$ GeV, while $R_{D^*}(q^2) < 1$ in the physical kinematic region. Additionally, we find that $R_M(q^2)$ increases monotonically with q^2 . This means that the decreasing rate of $d\Gamma_M^{\ell'}/dq^2$ in q^2 is faster than that of $d\Gamma_M^\tau/dq^2$. To see how sensitive $R_M(q^2)$ is to new physics effects, we show the results using benchmarks of $y_{L3}^q y_{R2}^u = -0.5$ (dashed) and $y_{L3}^q y_{R2}^u = -1$ (dot dashed) for $R_D(q^2)$ and $R_{D^*}(q^2)$ in the corresponding plots. We also consider the quantity $(R_M^{\text{NP}}(q^2) - R_M^{\text{SM}}(q^2))/R_M^{\text{SM}}(q^2)$ to exhibit the deviation caused by the new physics effects in $R_M(q^2)$ from the SM prediction, and the results are shown in Fig. 8. The variations of these curves show that $R_D(q^2)$ is more sensitive to new physics than $R_{D^*}(q^2)$ in the model.

TABLE III. Branching ratios of the $B^- \rightarrow D^{0(*)}\ell\nu$ decays in the SM and their experimental measurements.

Mode	$B^- \rightarrow D^0\ell\nu$	$B^- \rightarrow D\tau\nu$	$B^- \rightarrow D^{0*}\ell\nu$	$B^- \rightarrow D^{0*}\tau\nu$
SM	2.32%	6.89×10^{-3}	5.84%	1.50%
Exp [103]	$(2.30 \pm 0.09)\%$	$(7.7 \pm 2.5) \times 10^{-3}$	$(5.58 \pm 0.22)\%$	$(1.88 \pm 0.20)\%$

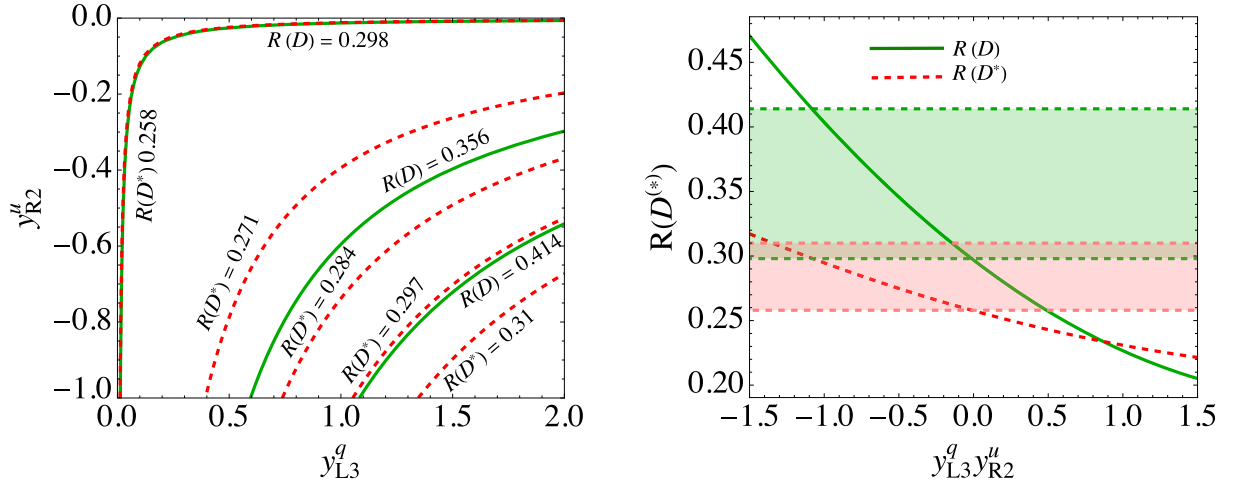


FIG. 6. Left: contours of $R(D)$ and $R(D^*)$ in the $y_{L3}^q - y_{R2}^u$ plane. The solid (darker green) and dashed (red) lines cover the 2σ range of the world-averaged $R(D)$ and $R(D^*)$, respectively. Right: dependence of $R(D^*)$ on $y_{L3}^q y_{R2}^u$. The light green [pink] shaded region represents the 2σ range of the world-averaged $R(D)$ [$R(D^*)$].

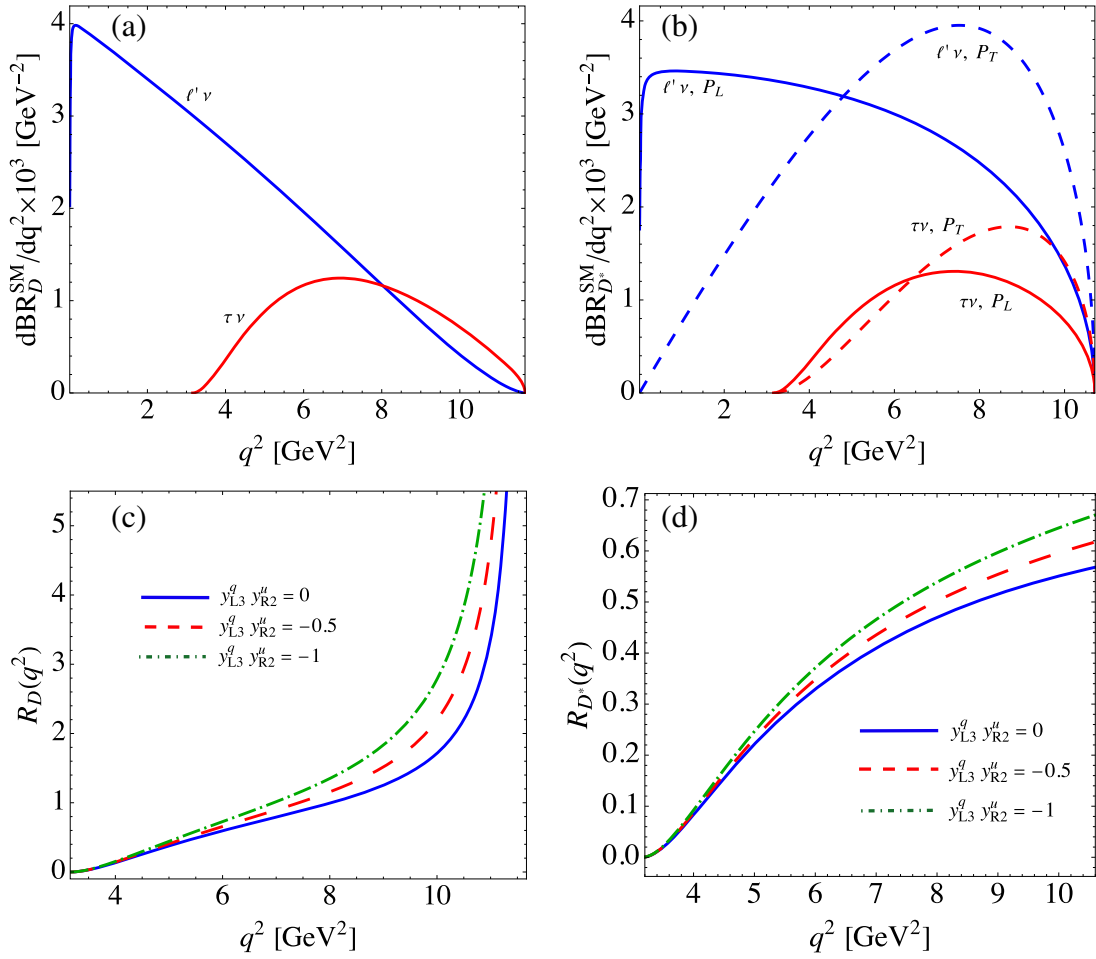


FIG. 7. Differential BR as a function of q^2 in the SM for (a) $B^- \rightarrow D^0 \ell' \nu$ and (b) $B^- \rightarrow D^* \ell' \nu$, where the longitudinal and transverse polarizations of D^* are illustrated separately. The ratios $R_D(q^2)$ (c) and $R_{D^*}(q^2)$ (d) as functions of q^2 , where the solid, dashed, and dot-dashed curves are plotted for $y_{L3}^q y_{R2}^u = 0, -0.5, \text{ and } -1$, respectively.

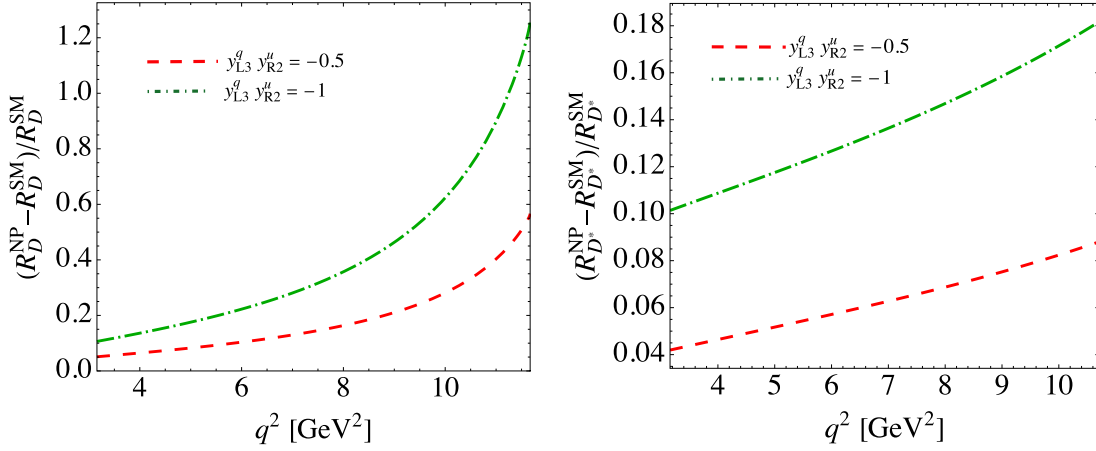


FIG. 8. Deviation of $R_M(q^2)$ from the SM result for $B^- \rightarrow D^0 \ell \nu$ (left) and $B^- \rightarrow D^{0*} \ell \nu$ (right).

3. The oblique parameters and W -mass

By combining the CDF II measurement of m_W with others, the oblique parameters are determined to be [110]

$$\begin{aligned} U &\equiv 0, & S &= 0.10 \pm 0.073, & T &= 0.202 \pm 0.056, \\ U &= 0.134 \pm 0.087, & S &= 0.05 \pm 0.096, & T &= 0.040 \pm 0.120. \end{aligned} \quad (68)$$

We can use these results to constrain the free parameters in the model. Based on Eqs. (B1), (B3), and (B4), the oblique parameters have a quadratic dependence on $c_{\beta-\alpha}$. However, $c_{\beta-\alpha} \lesssim \mathcal{O}(0.04)$ as previously discussed, meaning that its effects on the S , T , and U parameters are negligible. Therefore, these parameters can be approximated for the model as follows:

$$\begin{aligned} T &\simeq \frac{1}{16\alpha_{\text{em}}\pi^2 v^2} s_{\beta-\alpha}^2 F(m_{H^+}^2, m_H), \\ S &\simeq \frac{1}{24\pi} \left[(c_W^2 - s_W^2)^2 G(m_{H^+}^2, m_{H^+}^2, m_Z^2) + \ln \frac{m_{H^+}^2}{m_H^2} \right], \\ U &\simeq \frac{1}{24\pi} [s_{\beta-\alpha}^2 G(m_{H^+}^2, m_H^2, m_W^2) \\ &\quad - (2s_W^2 - 1)^2 G(m_{H^+}^2, m_{H^+}^2, m_Z^2)]. \end{aligned} \quad (69)$$

In this simplified form, the oblique parameters depend only on the ratio m_{H^+}/m_H . The contours for T (solid) and S (dashed) in the plane of m_{H^+} and m_H for the model are drawn in Fig. 9(a), where $s_{\beta-\alpha} \approx 1$ is taken in the estimates. Due to the fact that $U \ll T$, we do not show the results of U in the plot. The values of S and U in the model can only be up to the percent level and can be neglected in the numerical estimates for further phenomenological analyses. Thus, using the obtained T parameter, the loop-corrected W mass in the model is shown in Fig. 9(b), where the contours correspond to the central value, $\pm 2\sigma$ and $\pm 5\sigma$ of the world

average of $m_W = 80.4133 \pm 0.0080$ [110]. We observe that m_W increases with m_{H^+} for a given m_H , while a lower m_H is needed to increase m_W when m_{H^+} is fixed. For instance, $m_W \approx 80.43$ GeV can be achieved for $m_H \approx 50$ GeV and $m_{H^+} \approx 150$ GeV.

4. Z_1 and H decays

Finally, let's discuss possible decays of the light Z_1 and H . Because the mass of the light gauge boson is limited in the region of $m_{Z_1} \in (10, 100)$ MeV, it can only decay dominantly into on-shell light leptons through two-body decays. The Z_1 partial decay rate for possible final leptons is given by

$$\Gamma(Z_1 \rightarrow f\bar{f}) \simeq \frac{g^2 m_{Z_1}}{96c_W^2} (|C_R^f|^2 + |C_L^f|^2), \quad (70)$$

where $C_{R(L)}^f = C_{1V}^f \mp C_{1A}^f$, f denotes the possible light leptons (such as the three active neutrinos and the electron), and $m_f^2/m_{Z_1}^2 \approx 0$ is applied. The effective couplings of $C_{R,L}^f$ for each involved f are given as follows:

$$\begin{aligned} C_R^{\nu_e} &= 0, & C_L^{\nu_e} &= s_{\theta_z}, \\ C_L^{\nu_{\mu,\tau}} &= s_{\theta_z} \pm \frac{c_W m_{Z_1} c_{\theta_z}}{gv} \sqrt{2 + t_\beta^2 + t_\beta^{-2}}, \\ C_R^e &= 2s_W^2 s_{\theta_z}, & C_L^e &= (-1 + 2s_W^2) s_{\theta_z}. \end{aligned} \quad (71)$$

Although Z' does not couple to the first-generation leptons, the physical Z_1 can decay to them via $Z' - Z$ mixing.

If s_{θ_z} were not significantly smaller than $g_{Z'}$, the decay rates for $Z_1 \rightarrow (\bar{\nu}_e \nu_e, e^- e^+)$ could be sizable compared to the $Z_1 \rightarrow \bar{\nu}_{\ell'} \nu_{\ell'}$ decays. However, due to the large t_β enhancement in the Z_1 gauge coupling to $\nu_{\mu,\tau}$, the dominant decay channels are $Z_1 \rightarrow \nu_\mu \bar{\nu}_\mu / \nu_\tau \bar{\nu}_\tau$, with estimated BRs of approximately 50.5% and 49.5%, respectively. The BRs for $\nu_e \bar{\nu}_e$ and $e^- e^+$ as functions of t_β are presented in Fig. 10(a).

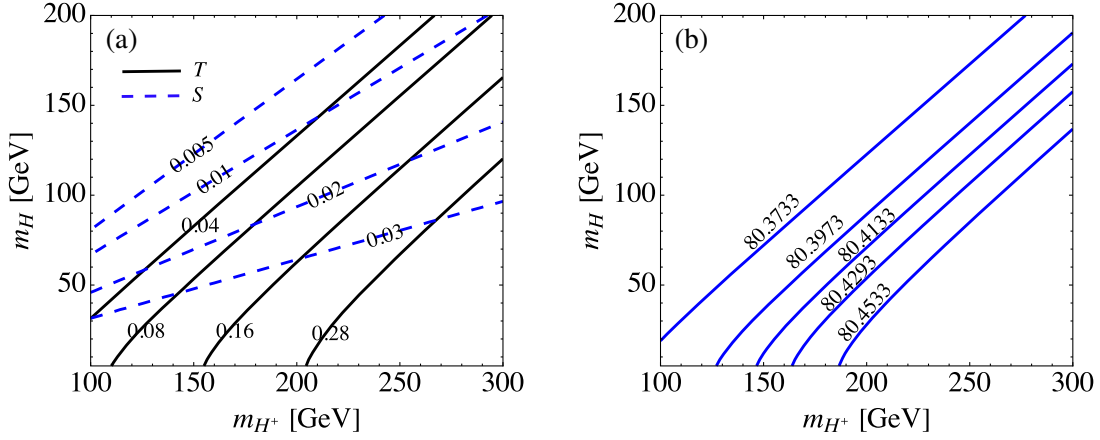


FIG. 9. (a) Contours of the oblique parameters, S and T , in the m_H - m_{H^+} plane. (b) Contours of m_W in the m_H - m_{H^+} plane.

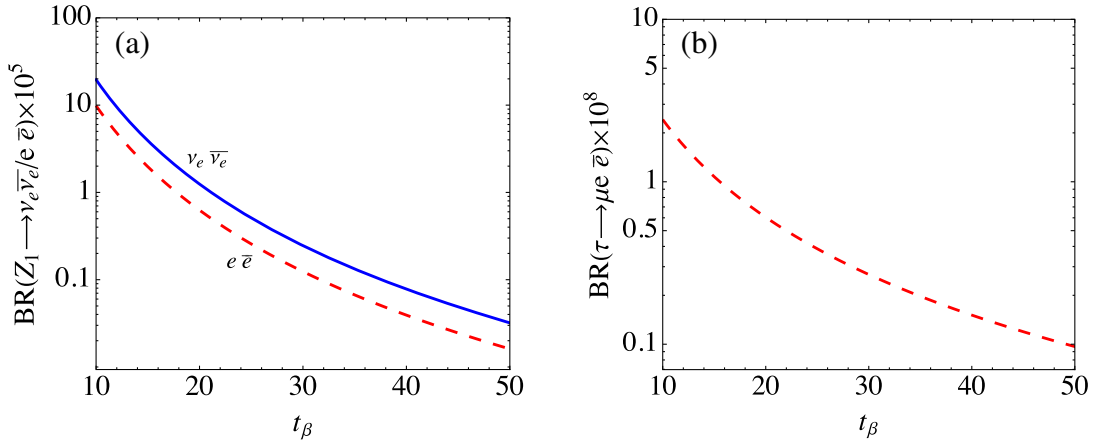


FIG. 10. BRs for (a) $Z_1 \rightarrow (\nu_e \bar{\nu}_e, e \bar{e})$ and (b) $\tau \rightarrow \mu Z_1 \rightarrow \mu e^- e^+$ as functions of t_β .

It is found that the BRs are more sensitive to t_β and less sensitive to m_{Z_1} . Because Z_1 can be produced in the $\tau \rightarrow \mu Z_1$ decay, which depends on the lepton flavor mixing θ_L , a significant $\text{BR}(Z_1 \rightarrow e^- e^+)$ thus implies a large BR for the LFV process $\tau \rightarrow \mu Z_1 \rightarrow \mu e^- e^+$, where the current upper limit is $\text{BR}(\tau \rightarrow \mu e^- e^+) < 1.8 \times 10^{-8}$ [103]. Our estimate of $\text{BR}(\tau \rightarrow \mu e^- e^+)$ is shown in Fig. 10(b), where $\chi_{\mu\tau} = 10^{-5}$ is used. Since $\tau \rightarrow \mu Z_1$ is also not sensitive to m_{Z_1} , the dependence of m_{Z_1} in $\text{BR}(\tau \rightarrow \mu e^- e^+)$ is not manifest. Assuming the integrated luminosity of 50 ab^{-1} , Belle II will be capable of probing the LFV process BRs down to the level of 10^{-10} – 10^{-9} [111]. The BR of $\mathcal{O}(10^{-9})$ for $\tau \rightarrow \mu e^- e^+$ predicted in this model can thus be probed at Belle II.

As discussed earlier, when $m_H < m_h/2$, H can be produced through the $h \rightarrow HH$ decay. The partial decay width of this process can provide a strict limit on the t_β and $c_{\beta-\alpha}$ parameters. In the following, we concentrate on this scenario, even though H generally can be heavier.

For two-body decays, H should decay into a pair of fermions, as long as the phase space permits. From

Eq. (25), its Yukawa couplings to fermions are suppressed by m_f/v and $(c_{\beta-\alpha} - s_{\beta-\alpha}/t_\beta)$, with no other factors that can enhance the partial decay width. As a result, $\Gamma(H \rightarrow f\bar{f})$ is small and negligible. However, even though suppressed by $m_{Z_1}^2/v$ from the gauge coupling as shown in

$$\mathcal{L}_{HZ_1 Z_1} \simeq \frac{2(t_\beta^2 - 1)}{t_\beta} \frac{m_{Z_1}^2}{v} s_{\beta-\alpha} \frac{HZ_1 \mu Z_1^\mu}{2}, \quad (72)$$

the $H \rightarrow Z_1 Z_1$ decay rate can be enhanced by the longitudinal component, which is proportional to $1/m_{Z_1}$. This leads to a partial decay width,

$$\Gamma(H \rightarrow Z_1 Z_1) \simeq \frac{m_H m_H^2}{32\pi v^2} \left| \frac{t_\beta^2 - 1}{t_\beta} s_{\beta-\alpha} \right|^2. \quad (73)$$

The original suppression factor from the gauge coupling is seen to be canceled by the longitudinal effect of $1/m_{Z_1}^2$ from each Z_1 boson. With $m_H = 50 \text{ GeV}$ and $t_\beta = 20$, we

obtain $\Gamma(H \rightarrow Z_1 Z_1) \approx 8.2 \text{ GeV}$. The other decay processes are subdominant. For example, the $H \rightarrow Z_1 Z_2^* \rightarrow Z_1 f \bar{f}$ decay has additional suppression factors due to the phase space and $1/m_{Z_2}^2$. An explicit estimate shows that the partial width for $H \rightarrow Z_1 Z_2^*$ is of $\mathcal{O}(10^{-5}) \text{ GeV}$. According to the earlier analysis, $Z_1 \rightarrow \nu \bar{\nu}$ is the dominant decay channel. Consequently, H predominantly decays into invisible neutrinos and becomes missing energy in the detector.

We now turn to the production of H at the LHC. First, H could be singly produced according to Eq. (22) via the vector boson fusion (VBF) process, but the $W^- W^+ (ZZ) H$ coupling is suppressed by $c_{\beta-\alpha}$. Additionally, the Yukawa coupling for the bremsstrahlung production of H with the top quark is determined by $(m_t/v)(c_{\beta-\alpha} - s_{\beta-\alpha}/t_\beta)$ and is also suppressed. However, H can be pair produced more copiously through the hHH and $W^- H^+ H$ couplings. In the former case, the H pair is produced by the on-shell Higgs boson; i.e., $pp \rightarrow h \rightarrow HH$. From Eq. (51), although $\Gamma(h \rightarrow HH)$ is associated with the small factor ξ , its BR can still be at the percent level. This amounts to the invisible decay of the Higgs boson [112]. In the latter case, the $W^- H^+ H$ coupling, as given in Eq. (22), is determined by the gauge coupling g with $s_{\beta-\alpha} \approx 1$. When H^+ is taken as an intermediate state in the t -channel scattering, H pair production occurs via the VBF channel, i.e., $pp \rightarrow HH + \text{forward jets}$. We may probe such an effect via the search for invisible decays of the new Higgs boson H [112].

V. SUMMARY

A sub-GeV Z' gauge boson has received much attention recently in the literature due to its distinctive characteristics, which could potentially resolve the observed anomalies, such as the muon $g-2$, and serve as a messenger between visible and dark sectors. Additionally, a light Z' gauge boson can make a significant contribution to $\text{CE}\nu\text{NS}$, as recently observed by the COHERENT experiment. Accordingly, we investigate the phenomenological impacts on flavor physics when the light Z' gauge boson originates from the local $U(1)_{L_\mu-L_\tau}$ gauge symmetry.

We have found that when a second Higgs doublet carrying the $U(1)_{L_\mu-L_\tau}$ charge is introduced to spontaneously break the $U(1)_{L_\mu-L_\tau}$ gauge symmetry, the new neutral and charged scalars can result in a larger W mass. Moreover, when a scalar leptoquark $S_3^\dagger = (\bar{3}, 1, 2/3)$ is added to the model, it would couple to the third-generation leptons in a unique way due to the $U(1)_{L_\mu-L_\tau}$ symmetry so that the branching ratios of $B \rightarrow (D, D^*) \tau \nu_\tau$ are enhanced, thus solving the $R(D)$ and $R(D^*)$ anomalies.

With the new Higgs doublet, the mixing between the new scalar boson and the SM-like Higgs leads to new decay channels for the Higgs boson, including

$h \rightarrow \mu\tau/Z_1 Z_1/Z_1 Z_2$ (and $h \rightarrow HH$ when $m_H < m_h/2$). It is found that due to the enhancement of $1/m_{Z_1}^2$, the $\tau \rightarrow \mu Z_1$ decay strictly constrains the $\mu - \tau$ flavor mixing, resulting in a highly suppressed $h \rightarrow \mu\tau$ decay. By assuming proper partial widths to the new Higgs decay channels, the $\tan\beta$ and $\cos(\beta - \alpha)$ parameters are limited, and the large $\tan\beta$ scheme is favored. Although the $\mu - \tau$ flavor-changing coupling is restricted to be small, the $\tau \rightarrow \mu Z_1 \rightarrow \mu e^- e^+$ decay, induced through the $Z - Z'$ mixing, can still reach the sensitivity of $\mathcal{O}(10^{-9})$ at Belle II.

Taking into account all potential constraints, we have found that the cross section of $\text{CE}\nu\text{NS}$ induced by the $Z' - Z$ mixing depends solely on the light gauge boson mass, m_{Z_1} . The mass region of m_{Z_1} that is used to fit the $\text{CE}\nu\text{NS}$ cross section, measured by COHERENT using the CsI target [3], can also explain the muon $g-2$ anomaly within 3σ . To demonstrate the sensitivity of new physics to $\text{CE}\nu\text{NS}$ in the model, we propose to study the cross section as a function of the incident neutrino energy. Our results show that in the low energy region, such as $E_\nu \sim 10 \text{ MeV}$, the deviation from the SM can exceed 15%, depending on the value of m_{Z_1} . To compare with results from other $U(1)$ gauge symmetries, we have examined the influence on the $\text{CE}\nu\text{NS}$ cross section from selected $U(1)$ gauged models, such as the universal, $B - L$, $B - 3L_\mu$, and $L_\mu - L_\tau$ with kinetic mixing. It has been found that only the model with dynamical $U(1)_{L_\mu-L_\tau}$ breaking can explain the anomaly of muon $g-2$ when the 1σ upper limits of the COHERENT data are imposed.

In addition to explaining the observed excesses in $R(D)$ and $R(D^*)$ using the introduced leptoquark, we have proposed a q^2 -dependent ratio of $d\Gamma/dq^2(B \rightarrow M\tau\nu)$ to the averaged differential decay rate of the light leptons $d\Gamma/dq^2(B \rightarrow M\ell'\nu)$, denoted by $R_M(q^2)$. Our results show that in the high q^2 region, $R_D(q^2)$ is more sensitive to the new physics effects and exhibits a significant deviation from the SM.

We have also studied the impact of the two-Higgs-doublet model on the oblique parameters and their relations to the W boson mass. With the approximation that $\cos(\beta - \alpha) \ll 1$, the parameters involved in the oblique parameters are m_H and m_{H^+} . We find a significant space in the $m_H - m_{H^+}$ plane that allows an enhancement of m_W up to the value observed by CDF II. Finally, we have discussed the possible decay channels for Z_1 and H in the scenario where $m_{Z_1} \in (10, 100) \text{ MeV}$ and $m_H < m_h/2$. The analysis shows that $Z_1 \rightarrow \nu_\mu \bar{\nu}_\mu / \nu_\tau \bar{\nu}_\tau$ and $H \rightarrow Z_1 Z_1$ are the dominant decay channels.

ACKNOWLEDGMENTS

This work was supported in part by the National Science and Technology Council, Taiwan under Grants No. MOST-110-2112-M-006-010-MY2 (C. H. C.) and MOST-111-2112-M-002-018-MY3 (C. W. C. and C. W. S.).

APPENDIX A: $\bar{B} \rightarrow D^{(*)}$ TRANSITION FORM FACTORS

1. Form factor parametrization

In this section, we define the $\bar{B} \rightarrow D^{(*)}$ transition form factors for the $\bar{B} \rightarrow D^{(*)}\ell\nu$ decays. First, the transition form factors associated with the various currents mediating the $\bar{B} \rightarrow D$ transitions are parametrized as

$$\begin{aligned}\langle D(p_2)|qb|\bar{B}(p_1)\rangle &= (m_B + m_D)F_S(q^2), \\ \langle D(p_2)|q\gamma^\mu b|\bar{B}(p_1)\rangle &= F_+(q^2)\left((p_1 + p_2)^\mu - \frac{m_B^2 - m_D^2}{q^2}q^\mu\right) + \frac{m_B^2 - m_D^2}{q^2}q^\mu F_0(q^2), \\ \langle D(p_2)|q\sigma_{\mu\nu}b|\bar{B}(p_1)\rangle &= -i(p_{1\mu}p_{2\nu} - p_{1\nu}p_{2\mu})\frac{2F_T(q^2)}{m_B + m_D},\end{aligned}\quad (\text{A1})$$

where the momentum transfer $q = p_1 - p_2$. For the $\bar{B} \rightarrow D^*$ transitions, the form factors are parametrized as

$$\begin{aligned}\langle D^*(p_2, \epsilon)|\bar{q}\gamma_\mu b|\bar{B}(p_1)\rangle &= i\epsilon_{\mu\nu\rho\sigma}\epsilon^{\nu*}p_1^\rho p_2^\sigma \frac{2V(q^2)}{m_B + m_{D^*}}, \\ \langle D^*(p_2, \epsilon)|\bar{q}\gamma_5 b|\bar{B}(p_1)\rangle &= -\frac{2m_{D^*}}{m_B + m_{D^*}}F_P(q^2)\epsilon^* \cdot q, \\ \langle D^*(p_2, \epsilon)|\bar{q}\gamma_\mu\gamma_5 b|\bar{B}(p_1)\rangle &= 2m_{D^*}A_0(q^2)\frac{\epsilon^* \cdot q}{q^2}q_\mu + (m_B + m_{D^*})A_1(q^2)\left(\epsilon_\mu^* - \frac{\epsilon^* \cdot q}{q^2}q_\mu\right) \\ &\quad - A_2(q^2)\frac{\epsilon^* \cdot q}{m_B + m_{D^*}}\left((p_1 + p_2)_\mu - \frac{m_B^2 - m_{D^*}^2}{q^2}q_\mu\right), \\ \langle D^*(p_2, \epsilon)|\bar{q}\sigma_{\mu\nu}b|\bar{B}(p_1)\rangle &= \epsilon_{\mu\nu\rho\sigma}\left[\epsilon^{\rho*}(p_1 + p_2)^\sigma T_1(q^2) + \epsilon^{\rho*}q^\sigma \frac{m_B^2 - m_{D^*}^2}{q^2}(T_2(q^2) - T_1(q^2))\right. \\ &\quad \left. + 2\frac{\epsilon^* \cdot q}{q^2}p_1^\rho p_2^\sigma \left(T_2(q^2) - T_1(q^2) + \frac{q^2}{m_B^2 - m_{D^*}^2}T_3(q^2)\right)\right],\end{aligned}\quad (\text{A2})$$

where $\epsilon^{0123} \equiv 1$, $\sigma_{\mu\nu}\gamma_5 = \frac{i}{2}\epsilon_{\mu\nu\rho\sigma}\sigma^{\rho\sigma}$, and ϵ^μ denotes the polarization vector of the D^* meson.

2. Form factors in the HQET

To numerically estimate the BRs of the $\bar{B} \rightarrow D^{(*)}\ell\nu$ decays, a QCD approach is necessary to evaluate the involved form factors. In this study, we use the results presented in Ref. [59], which is based on the HQET. Since the parametrization of the form factors in the HQET differs from those in Eqs. (A1) and (A2), we introduce here the HQET notation and provide the relationship between the different parametrizations. We first define the dimensionless kinetic variables in the HQET:

$$v^\mu = \frac{p_B^\mu}{m_B}, \quad v'^\mu = \frac{p_{D^{(*)}}^\mu}{m_{D^{(*)}}}, \quad w = v \cdot v' = \frac{m_B^2 + m_{D^{(*)}}^2 - q^2}{2m_B m_{D^{(*)}}}.\quad (\text{A3})$$

The form factors for the $\bar{B} \rightarrow D$ transitions are then parametrized as [59]

$$\begin{aligned}\langle D|\bar{c}b|\bar{B}\rangle &= \sqrt{m_B m_D}h_S(w+1), \\ \langle D|\bar{c}\gamma^\mu b|\bar{B}\rangle &= \sqrt{m_B m_D}[h_+(v+v')^\mu + h_-(v-v')^\mu], \\ \langle D|\bar{c}\sigma^{\mu\nu}b|\bar{B}\rangle &= i\sqrt{m_B m_D}h_T(v'^\mu v^\nu - v'^\nu v^\mu),\end{aligned}\quad (\text{A4})$$

and those for the $\bar{B} \rightarrow D^*$ transitions are

$$\begin{aligned}\langle D^*|\bar{c}\gamma^5 b|\bar{B}\rangle &= -\sqrt{m_B m_{D^*}}h_P\epsilon^* \cdot v, \\ \langle D^*|\bar{c}\gamma^\mu b|\bar{B}\rangle &= i\sqrt{m_B m_{D^*}}h_V\epsilon^{\mu\alpha\beta}\epsilon_\alpha^*v'_\beta, \\ \langle D^*|\bar{c}\gamma^\mu\gamma^5 b|\bar{B}\rangle &= \sqrt{m_B m_{D^*}}[h_{A_1}(w+1)\epsilon^{*\mu} - h_{A_2}(\epsilon^* \cdot v)v^\mu \\ &\quad - h_{A_3}(\epsilon^* \cdot v)v'^\mu], \\ \langle D^*|\bar{c}\sigma^{\mu\nu}b|\bar{B}\rangle &= -\sqrt{m_B m_{D^*}}[h_{T_1}\epsilon_\alpha^*(v+v')_\beta + h_{T_2}\epsilon_\alpha^* \\ &\quad \times (v-v')_\beta + h_{T_3}(\epsilon^* \cdot v)v_\alpha v'_\beta],\end{aligned}\quad (\text{A5})$$

where h_- , h_{A_2} , and $h_{T_{2,3}}$ vanish in the heavy quark limit, and the remaining form factors are equal to the leading-order Isgur-Wise function $\xi(w)$.

We take the parametrization of the leading-order Isgur-Wise function as [113]:

$$\frac{\xi(w)}{\xi(w_0)} \simeq 1 - 8a^2\bar{\rho}_*^2 z_* + [V_{21}\bar{\rho}_*^2 - V_{20} + \Delta(e_b, e_c, \alpha_s)]z_*^2, \quad (\text{A6})$$

where $V_{21} = 57.0$, $V_{20} = 7.5$, z_* and a are defined as [113]

$$z_* = \frac{\sqrt{w+1} - \sqrt{2}a}{\sqrt{w+1} + \sqrt{2}a}, \quad a = \sqrt{\frac{1+r_D}{2\sqrt{r_D}}}, \quad (\text{A7})$$

$r_D = m_D/m_B$, w_0 is determined from solving $z_*(w_0) = 0$, $\bar{\rho}_*^2$ is the slope parameter of $\xi(w)/\xi(w_0)$, and $\Delta(e_b, e_c, \alpha_s)$ denotes the correction effects of $\mathcal{O}(e_{b,c})$ with $e_{b(c)} = \bar{\Lambda}/m_{b(c)}$ and $\mathcal{O}(\alpha_s)$. For numerical estimates, we take the results from the fit scenario of “ $L_{w \geq 1} + \text{SR}$ ” shown in [59]. In addition to $\bar{\rho}_*^2 = 1.24 \pm 0.08$, the values of subleading Isgur-Wise functions at $w = 1$ are given in Table IV. Using these results, the correction of $\mathcal{O}(e_{b,c})$ and $\mathcal{O}(\alpha_s)$ can be obtained as

$$\Delta(e_b, e_c, \alpha_s) \approx 0.582 \pm 0.298, \quad (\text{A8})$$

where we take the 1S scheme for m_b and $m_b^{1S} = 4.71 \pm 0.05$ GeV [59]. In addition, $\delta m_{bc} = m_b - m_c = 3.40 \pm 0.02$ GeV and $\bar{\Lambda} = 0.45$ GeV are used.

Hence, the form factors up to $\mathcal{O}(e_{b,c})$ and $\mathcal{O}(\alpha_s)$ can be expressed by factoring out ξ ; i.e., $h_i = \hat{h}_i \xi$, where \hat{h}_i for the $\bar{B} \rightarrow D$ transitions are given by [59]

$$\hat{h}_+ = 1 + \hat{\alpha}_s \left[C_{V_1} + \frac{w+1}{2} (C_{V_1} + C_{V_3}) \right] + (e_c + e_b) \hat{L}_1, \quad (\text{A9a})$$

$$\hat{h}_- = \hat{\alpha}_s \frac{w+1}{2} (C_{V_2} - C_{V_3}) + (e_c - e_b) \hat{L}_4, \quad (\text{A9b})$$

$$\hat{h}_S = 1 + \hat{\alpha}_s C_S + (e_c + e_b) \left[\hat{L}_1 - \hat{L}_4 \frac{w-1}{w+1} \right], \quad (\text{A9c})$$

$$\hat{h}_T = 1 + \hat{\alpha}_s (C_{T_1} - C_{T_2} + C_{T_3}) + (e_c + e_b) (\hat{L}_1 - \hat{L}_4), \quad (\text{A9d})$$

and those for the $\bar{B} \rightarrow D^*$ transitions are given by

$$\hat{h}_V = 1 + \alpha_s C_{V_1} + e_c (\hat{L}_2 - \hat{L}_5) + e_b (\hat{L}_1 - \hat{L}_4), \quad (\text{A10a})$$

$$\hat{h}_{A_1} = 1 + \hat{\alpha}_s C_{A_1} + e_c \left(\hat{L}_2 - \hat{L}_5 \frac{w-1}{w+1} \right) + e_b \left(\hat{L}_1 - \hat{L}_4 \frac{w-1}{w+1} \right), \quad (\text{A10b})$$

$$\hat{h}_{A_2} = \hat{\alpha}_s C_{A_2} + e_c (\hat{L}_3 + \hat{L}_6), \quad (\text{A10c})$$

$$\hat{h}_{A_3} = 1 + \hat{\alpha}_s (C_{A_1} + C_{A_3}) + e_c (\hat{L}_2 - \hat{L}_3 + \hat{L}_6 - \hat{L}_5) + e_b (\hat{L}_1 - \hat{L}_4), \quad (\text{A10d})$$

$$\hat{h}_P = 1 + \hat{\alpha}_s C_P + e_c [\hat{L}_2 + \hat{L}_3(w-1) + \hat{L}_5 - \hat{L}_6(w+1)] + e_b (\hat{L}_1 - \hat{L}_4), \quad (\text{A10e})$$

$$\hat{h}_{T_1} = 1 + \hat{\alpha}_s \left[C_{T_1} + \frac{w-1}{2} (C_{T_2} - C_{T_3}) \right] + e_c \hat{L}_2 + e_b \hat{L}_1, \quad (\text{A10f})$$

$$\hat{h}_{T_2} = \hat{\alpha}_s \frac{w+1}{2} (C_{T_2} + C_{T_3}) + e_c \hat{L}_5 - e_b \hat{L}_4, \quad (\text{A10g})$$

$$\hat{h}_{T_3} = \hat{\alpha}_s C_{T_2} + e_c (\hat{L}_6 - \hat{L}_3). \quad (\text{A10h})$$

The w -dependent functions C_{Γ_i} can be found in Ref. [114], and the subleading Isgur-Wise functions are [115]

$$\begin{aligned} \hat{L}_1 &= -4(w-1)\hat{\chi}_2 + 12\hat{\chi}_3, & \hat{L}_2 &= -4\hat{\chi}_3, & \hat{L}_3 &= 4\hat{\chi}_2, \\ \hat{L}_4 &= 2\eta - 1, & \hat{L}_5 &= -1, & \hat{L}_6 &= -2\frac{1+\eta}{w+1}, \end{aligned} \quad (\text{A11})$$

where the w -dependent functions $\hat{\chi}_i$ and η can be approximated as

$$\begin{aligned} \hat{\chi}_2(w) &\simeq \hat{\chi}_2(1) + \hat{\chi}'_2(1)(w-1), \\ \hat{\chi}_3(w) &\simeq \hat{\chi}'_3(1)(w-1), \\ \eta(w) &\simeq \eta(1) + \eta'(1)(w-1). \end{aligned} \quad (\text{A12})$$

The form factor parametrizations in Eqs. (A1) and (A2), using which we formulate the BRs, and in Eqs. (A4) and (A5), for which we evaluate within the framework of the HQET, are related as follows:

TABLE IV. The results of subleading Isgur-Wise functions from the “ $L_{w \geq 1} + \text{SR}$ ” fit scenario.

FS	$\hat{\chi}_2(1)$	$\hat{\chi}'_2(1)$	$\hat{\chi}'_3(1)$	$\eta(1)$	$\eta'(1)$
$L_{w \geq 1} + \text{SR}$	-0.06 ± 0.02	-0.00 ± 0.02	0.05 ± 0.02	0.30 ± 0.03	-0.05 ± 0.09

$$\begin{aligned}
F_S(q^2) &= \frac{\sqrt{m_B m_D}}{m_B + m_D} (w-1) h_S(w), \\
F_+(q^2) &= \frac{1}{2\sqrt{m_B m_D}} [(m_B + m_D) h_+(w) \\
&\quad - (m_B - m_D) h_-(w)], \\
F_0(q^2) &= \frac{1}{2\sqrt{m_B m_D}} \left[\frac{(m_B + m_D)^2 - q^2}{m_B + m_D} h_+(w) \right. \\
&\quad \left. - \frac{(m_B - m_D)^2 - q^2}{m_B - m_D} h_-(w) \right], \\
F_T(q^2) &= \frac{m_B + m_D}{2\sqrt{m_B m_D}} h_T(w). \tag{A13}
\end{aligned}$$

The relations for the form factors arising from the pseudoscalar, vector, and axial-vector currents for the $\bar{B} \rightarrow D^*$ transitions are found to be

$$\begin{aligned}
F_P(q^2) &= \frac{m_B + m_{D^*}}{2\sqrt{m_B m_{D^*}}} h_P(w), \\
V(q^2) &= \frac{m_B + m_{D^*}}{2\sqrt{m_B m_{D^*}}} h_V(w), \\
A_0(q^2) &= \frac{1}{2\sqrt{m_B m_{D^*}}} \left[\frac{(m_B + m_{D^*})^2 - q^2}{2m_{D^*}} h_{A_1}(w) \right. \\
&\quad \left. - \frac{m_B^2 - m_{D^*}^2 + q^2}{2m_B} h_{A_2}(w) - \frac{m_B^2 - m_{D^*}^2 - q^2}{2m_{D^*}} h_{A_3}(w) \right], \\
A_1(q^2) &= \frac{(m_B + m_{D^*})^2 - q^2}{2\sqrt{m_B m_{D^*}} (m_B + m_{D^*})} h_{A_1}(w), \\
A_2(q^2) &= \frac{m_B + m_{D^*}}{2\sqrt{m_B m_{D^*}}} \left(h_{A_3}(w) + \frac{m_{D^*}}{m_B} h_{A_2}(w) \right). \tag{A14}
\end{aligned}$$

Finally, the tensor form factors for the $\bar{B} \rightarrow D^*$ transitions are related by

$$\begin{aligned}
T_1(q^2) &= \frac{1}{2\sqrt{m_B m_{D^*}}} [(m_B + m_{D^*}) h_{T_1}(w) \\
&\quad - (m_B - m_{D^*}) h_{T_2}(w)], \\
T_2(q^2) &= \frac{1}{2\sqrt{m_B m_{D^*}}} \left[\frac{(m_B + m_{D^*})^2 - q^2}{m_B + m_{D^*}} h_{T_1}(w) \right. \\
&\quad \left. - \frac{(m_B - m_{D^*})^2 - q^2}{m_B - m_{D^*}} h_{T_2}(w) \right], \\
T_3(q^2) &= \frac{1}{2\sqrt{m_B m_{D^*}}} \left[(m_B - m_{D^*}) h_{T_1}(w) \right. \\
&\quad \left. - (m_B + m_{D^*}) h_{T_2}(w) + \frac{m_B^2 - m_{D^*}^2}{m_B} h_{T_3}(w) \right]. \tag{A15}
\end{aligned}$$

APPENDIX B: OBLIQUE PARAMETERS IN THE MODEL

To calculate the S , T , and U parameters in the model, we apply the results obtained in Ref. [96]. Using the mixing matrices of Goldstone and scalar bosons shown in Eqs. (9) and (13), the resulting T parameter subtracting the SM result is expressed as

$$\begin{aligned}
\alpha_{\text{em}} T &= \frac{1}{16\pi^2 v^2} \{ c_{\beta-\alpha}^2 F(m_{H^+}^2, m_h^2) + s_{\beta-\alpha}^2 F(m_{H^+}^2, m_H^2) \\
&\quad + 3c_{\beta-\alpha}^2 [F(m_Z^2, m_H^2) - F(m_W^2, m_H^2)] \\
&\quad - F(m_Z^2, m_h^2) + F(m_W^2, m_h^2) \}, \tag{B1}
\end{aligned}$$

where $\alpha_{\text{em}} = e^2/4\pi$ is the fine structure constant of QED, and the function F is defined as

$$F(m_a^2, m_b^2) = \frac{m_a^2 + m_b^2}{2} - \frac{m_a^2 m_b^2}{m_a^2 - m_b^2} \ln \frac{m_a^2}{m_b^2}. \tag{B2}$$

In the limit of $s_{\beta-\alpha} \rightarrow 1$, the H^\pm - and H -mediated loop effects are the most dominant.

The S and U parameters are respectively given by

$$\begin{aligned}
S &= \frac{1}{24\pi} \left[(c_W^2 - s_W^2)^2 G(m_{H^+}^2, m_{H^+}^2, m_Z^2) + \ln \frac{m_{H^+}^2}{m_H^2} \right. \\
&\quad \left. + c_{\beta-\alpha}^2 (\hat{G}(m_H^2, m_Z^2) - \hat{G}(m_h^2, m_Z^2)) \right], \tag{B3}
\end{aligned}$$

and

$$\begin{aligned}
U &= \frac{1}{24\pi} [c_{\beta-\alpha}^2 G(m_{H^+}^2, m_h^2, m_W^2) + s_{\beta-\alpha}^2 G(m_{H^+}^2, m_H^2, m_W^2) \\
&\quad - (2s_W^2 - 1)^2 G(m_{H^+}^2, m_{H^+}^2, m_Z^2) \\
&\quad + c_{\beta-\alpha}^2 (\hat{G}(m_H^2, m_W^2) - \hat{G}(m_h^2, m_W^2)) \\
&\quad - \hat{G}(m_h^2, m_W^2) + \hat{G}(m_h^2, m_Z^2)], \tag{B4}
\end{aligned}$$

where the functions of G and \tilde{G} are given by

$$\begin{aligned}
G(m_a^2, m_b^2, m_c^2) &= -\frac{16}{3} + \frac{5(m_a^2 + m_b^2)}{m_c^2} - \frac{2(m_a^2 - m_b^2)^2}{m_c^4} \\
&\quad + \frac{r}{m_c^6} f(t, r) + \frac{3}{m_c^2} \left(\frac{m_a^4 + m_b^4}{m_a^2 - m_b^2} \right. \\
&\quad \left. - \frac{m_a^4 - m_b^4}{m_c^2} + \frac{(m_a^2 - m_b^2)^3}{3m_c^4} \right) \ln \frac{m_a^2}{m_b^2}, \tag{B5}
\end{aligned}$$

$$\begin{aligned}
\tilde{G}(m_a^2, m_b^2, m_c^2) &= -2 + \left(\frac{m_a^2 - m_b^2}{m_c^2} - \frac{m_a^2 + m_b^2}{m_a^2 - m_b^2} \right) \\
&\quad \times \ln \frac{m_a^2}{m_b^2} + \frac{f(t, r)}{m_c^2}, \tag{B6}
\end{aligned}$$

and \hat{G} , t , r , and $f(t, r)$ are defined as

$$\begin{aligned}\hat{G}(m_a^2, m_b^2) &= G(m_a^2, m_b^2, m_b^2) + 12\tilde{G}(m_a^2, m_b^2, m_b^2), \\ t &= m_a^2 + m_b^2 - m_c^2, \\ r &= m_c^4 - 2m_c^2(m_a^2 + m_b^2) + (m_a^2 - m_b^2)^2, \\ f(t, r) &= \begin{cases} \sqrt{r} \ln \left| \frac{t - \sqrt{r}}{t + \sqrt{r}} \right| & \text{for } r > 0, \\ 0 & \text{for } r = 0, \\ 2\sqrt{-r} \arctan \frac{\sqrt{-r}}{t} & \text{for } r < 0. \end{cases} \end{aligned} \quad (\text{B7})$$

-
- [1] D. Z. Freedman, *Phys. Rev. D* **9**, 1389 (1974).
[2] D. Akimov *et al.* (COHERENT Collaboration), *Science* **357**, 1123 (2017).
[3] D. Akimov *et al.* (COHERENT Collaboration), *Phys. Rev. Lett.* **129**, 081801 (2022).
[4] D. Akimov *et al.* (COHERENT Collaboration), *Phys. Rev. Lett.* **126**, 012002 (2021).
[5] P. Coloma, M. C. Gonzalez-Garcia, M. Maltoni, and T. Schwetz, *Phys. Rev. D* **96**, 115007 (2017).
[6] J. Liao and D. Marfatia, *Phys. Lett. B* **775**, 54 (2017).
[7] C. Giunti, *Phys. Rev. D* **101**, 035039 (2020).
[8] P. Coloma, I. Esteban, M. C. Gonzalez-Garcia, and M. Maltoni, *J. High Energy Phys.* **02** (2020) 023.
[9] P. B. Denton and J. Gehrlein, *J. High Energy Phys.* **04** (2021) 266.
[10] A. N. Khan, D. W. McKay, and W. Rodejohann, *Phys. Rev. D* **104**, 015019 (2021).
[11] M. Hoferichter, J. Menéndez, and A. Schwenk, *Phys. Rev. D* **102**, 074018 (2020).
[12] J. Liao, H. Liu, and D. Marfatia, *Phys. Rev. D* **106**, L031702 (2022).
[13] M. Abdullah, H. Abele, D. Akimov, G. Angloher, D. Aristizabal Sierra, C. Augier, A. B. Balantekin, L. Balogh, P. S. Barbeau, L. Baudis *et al.*, [arXiv:2203.07361](https://arxiv.org/abs/2203.07361).
[14] R. Calabrese, J. Gunn, G. Miele, S. Morisi, S. Roy, and P. Santorelli, *Phys. Rev. D* **107**, 055039 (2023).
[15] D. K. Papoulias and T. S. Kosmas, *Phys. Rev. D* **97**, 033003 (2018).
[16] M. Abdullah, J. B. Dent, B. Dutta, G. L. Kane, S. Liao, and L. E. Strigari, *Phys. Rev. D* **98**, 015005 (2018).
[17] P. B. Denton, Y. Farzan, and I. M. Shoemaker, *J. High Energy Phys.* **07** (2018) 037.
[18] A. Aguilar-Arevalo *et al.* (CONNIE Collaboration), *J. High Energy Phys.* **04** (2020) 054.
[19] O. G. Miranda, D. K. Papoulias, G. Sanchez Garcia, O. Sanders, M. Tórtola, and J. W. F. Valle, *J. High Energy Phys.* **05** (2020) 130; **01** (2021) 67(E).
[20] M. Cadeddu, N. Cargioli, F. Dordei, C. Giunti, Y. F. Li, E. Picciau, and Y. Y. Zhang, *J. High Energy Phys.* **01** (2021) 116.
[21] P. Coloma, M. C. Gonzalez-Garcia, and M. Maltoni, *J. High Energy Phys.* **01** (2021) 114; **11** (2022) 115(E).
[22] L. M. G. de la Vega, L. J. Flores, N. Nath, and E. Peinado, *J. High Energy Phys.* **09** (2021) 146.
[23] H. Bonet *et al.* (CONUS Collaboration), *J. High Energy Phys.* **05** (2022) 085.
[24] P. Coloma, I. Esteban, M. C. Gonzalez-Garcia, L. Larizgoitia, F. Monrabal, and S. Palomares-Ruiz, *J. High Energy Phys.* **05** (2022) 037.
[25] M. Atzori Corona, M. Cadeddu, N. Cargioli, F. Dordei, C. Giunti, Y. F. Li, E. Picciau, C. A. Ternes, and Y. Y. Zhang, *J. High Energy Phys.* **05** (2022) 109.
[26] X. G. He, G. C. Joshi, H. Lew, and R. R. Volkas, *Phys. Rev. D* **43**, 22 (1991).
[27] X. G. He, G. C. Joshi, H. Lew, and R. R. Volkas, *Phys. Rev. D* **44**, 2118 (1991).
[28] C. H. Chen and T. Nomura, *Phys. Rev. D* **96**, 095023 (2017).
[29] T. Aoyama, N. Asmussen, M. Benayoun, J. Bijnens, T. Blum, M. Bruno, I. Caprini, C. M. Carloni Calame, M. Cè, G. Colangelo *et al.*, *Phys. Rep.* **887**, 1 (2020).
[30] J. Heeck and W. Rodejohann, *Phys. Rev. D* **84**, 075007 (2011).
[31] T. Aaltonen *et al.* (CDF Collaboration), *Science* **376**, 170 (2022).
[32] T. A. Aaltonen *et al.* (CDF and D0 Collaborations), *Phys. Rev. D* **88**, 052018 (2013).
[33] ATLAS Collaboration, Improved W boson mass measurement using 7 TeV proton-proton collisions with the ATLAS detector, Report No. ATLAS-CONF-2023-004.
[34] S. Heinemeyer, W. Hollik, G. Weiglein, and L. Zeune, *J. High Energy Phys.* **12** (2013) 084.
[35] Y. Z. Fan, T. P. Tang, Y. L. S. Tsai, and L. Wu, *Phys. Rev. Lett.* **129**, 091802 (2022).
[36] A. Strumia, *J. High Energy Phys.* **08** (2022) 248.
[37] E. Bagnaschi, J. Ellis, M. Madigan, K. Mimasu, V. Sanz, and T. You, *J. High Energy Phys.* **08** (2022) 308.
[38] H. Bahl, J. Braathen, and G. Weiglein, *Phys. Lett. B* **833**, 137295 (2022).
[39] Y. Cheng, X. G. He, Z. L. Huang, and M. W. Li, *Phys. Lett. B* **831**, 137218 (2022).
[40] P. Asadi, C. Cesarotti, K. Fraser, S. Homiller, and A. Parikh, *Phys. Rev. D* **108**, 055026 (2023).

- [41] J. J. Heckman, *Phys. Lett. B* **833**, 137387 (2022).
- [42] A. Crivellin, M. Kirk, T. Kitahara, and F. Mescia, *Phys. Rev. D* **106**, L031704 (2022).
- [43] P. Fileviez Perez, H. H. Patel, and A. D. Plascencia, *Phys. Lett. B* **833**, 137371 (2022).
- [44] S. Kanemura and K. Yagyu, *Phys. Lett. B* **831**, 137217 (2022).
- [45] J. Kim, S. Lee, P. Sanyal, and J. Song, *Phys. Rev. D* **106**, 035002 (2022).
- [46] X. Q. Li, Z. J. Xie, Y. D. Yang, and X. B. Yuan, *Phys. Lett. B* **838**, 137651 (2023).
- [47] R. Dacruz and A. Thapa, *Phys. Rev. D* **107**, 015002 (2023).
- [48] T. A. Chowdhury and S. Saad, *Phys. Rev. D* **106**, 055017 (2022).
- [49] J. Gao, D. Liu, and K. Xie, *Chin. Phys. C* **46**, 123110 (2022).
- [50] X. F. Han, F. Wang, L. Wang, J. M. Yang, and Y. Zhang, *Chin. Phys. C* **46**, 103105 (2022).
- [51] Y. Cheng, X. G. He, F. Huang, J. Sun, and Z. P. Xing, *Nucl. Phys. B* **989**, 116118 (2023).
- [52] T. Bandyopadhyay, A. Budhraj, S. Mukherjee, and T. S. Roy, *J. High Energy Phys.* **08** (2023) 135.
- [53] C. H. Chen, C. W. Chiang, and C. W. Su, [arXiv:2301.07070](https://arxiv.org/abs/2301.07070).
- [54] J. Heeck, M. Holthausen, W. Rodejohann, and Y. Shimizu, *Nucl. Phys. B* **896**, 281 (2015).
- [55] J. Heeck, *Phys. Lett. B* **758**, 101 (2016).
- [56] J. A. Bailey *et al.* (MILC Collaboration), *Phys. Rev. D* **92**, 034506 (2015).
- [57] H. Na *et al.* (HPQCD Collaboration), *Phys. Rev. D* **92**, 054510 (2015); **93**, 119906(E) (2016).
- [58] D. Bigi and P. Gambino, *Phys. Rev. D* **94**, 094008 (2016).
- [59] F. U. Bernlochner, Z. Ligeti, M. Papucci, and D. J. Robinson, *Phys. Rev. D* **95**, 115008 (2017); **97**, 059902(E) (2018).
- [60] S. Jaiswal, S. Nandi, and S. K. Patra, *J. High Energy Phys.* **12** (2017) 060.
- [61] J. P. Lees *et al.* (BABAR Collaboration), *Phys. Rev. Lett.* **123**, 091801 (2019).
- [62] M. Bordone, M. Jung, and D. van Dyk, *Eur. Phys. J. C* **80**, 74 (2020).
- [63] G. Martinelli, S. Simula, and L. Vittorio, *Phys. Rev. D* **105**, 034503 (2022).
- [64] Y. S. Amhis *et al.* (Heavy Flavor Averaging Group and HFLAV Collaborations), *Phys. Rev. D* **107**, 052008 (2023).
- [65] R. Aaij *et al.* (LHCb Collaboration), *Phys. Rev. Lett.* **131**, 111802 (2023).
- [66] R. Aaij *et al.* (LHCb Collaboration), *Phys. Rev. D* **108**, 012018 (2023).
- [67] R. Aaij *et al.* (LHCb Collaboration), *Phys. Rev. Lett.* **120**, 121801 (2018).
- [68] R. Aaij *et al.* (LHCb Collaboration), *Phys. Rev. Lett.* **128**, 191803 (2022).
- [69] M. Fedele, M. Blanke, A. Crivellin, S. Iguro, T. Kitahara, U. Nierste, and R. Watanabe, *Phys. Rev. D* **107**, 055005 (2023).
- [70] A. Crivellin, C. Greub, and A. Kokulu, *Phys. Rev. D* **86**, 054014 (2012).
- [71] A. Crivellin, A. Kokulu, and C. Greub, *Phys. Rev. D* **87**, 094031 (2013).
- [72] A. Crivellin, J. Heeck, and P. Stoffer, *Phys. Rev. Lett.* **116**, 081801 (2016).
- [73] C. H. Chen and T. Nomura, *Eur. Phys. J. C* **77**, 631 (2017).
- [74] A. G. Akeroyd and C. H. Chen, *Phys. Rev. D* **96**, 075011 (2017).
- [75] C. H. Chen and T. Nomura, *Phys. Rev. D* **98**, 095007 (2018).
- [76] D. Bečirević, S. Fajfer, N. Košnik, and O. Sumensari, *Phys. Rev. D* **94**, 115021 (2016).
- [77] B. Bhattacharya, A. Datta, J. P. Guévin, D. London, and R. Watanabe, *J. High Energy Phys.* **01** (2017) 015.
- [78] A. Crivellin, J. Fuentes-Martin, A. Greljo, and G. Isidori, *Phys. Lett. B* **766**, 77 (2017).
- [79] A. Crivellin, D. Müller, and T. Ota, *J. High Energy Phys.* **09** (2017) 040.
- [80] C. H. Chen, T. Nomura, and H. Okada, *Phys. Lett. B* **774**, 456 (2017).
- [81] C. H. Chen and T. Nomura, *Phys. Lett. B* **777**, 420 (2018).
- [82] A. Crivellin, D. Müller, and F. Saturnino, *J. High Energy Phys.* **06** (2020) 020.
- [83] J. Heeck and A. Thapa, *Eur. Phys. J. C* **82**, 480 (2022).
- [84] I. Adachi *et al.* (Belle-II Collaboration), [arXiv:2311.14647](https://arxiv.org/abs/2311.14647).
- [85] C. H. Chen and C. W. Chiang, [arXiv:2309.12904](https://arxiv.org/abs/2309.12904).
- [86] K. G. Klimenko, *Theor. Math. Phys.* **62**, 58 (1985).
- [87] K. Kannike, *Eur. Phys. J. C* **72**, 2093 (2012).
- [88] U. Baur, T. Plehn, and D. L. Rainwater, *Phys. Rev. Lett.* **89**, 151801 (2002).
- [89] G. C. Branco, P. M. Ferreira, L. Lavoura, M. N. Rebelo, M. Sher, and J. P. Silva, *Phys. Rep.* **516**, 1 (2012).
- [90] S. Klein and J. Nystrand, *Phys. Rev. C* **60**, 014903 (1999).
- [91] P. S. Barbeau, Y. Efremenko, and K. Scholberg, [arXiv:2111.07033](https://arxiv.org/abs/2111.07033).
- [92] E. Bertuzzo, G. Grilli di Cortona, and L. M. D. Ramos, *J. High Energy Phys.* **06** (2022) 075.
- [93] I. Doršner, S. Fajfer, N. Košnik, and I. Nišandžić, *J. High Energy Phys.* **11** (2013) 084.
- [94] M. E. Peskin and T. Takeuchi, *Phys. Rev. Lett.* **65**, 964 (1990).
- [95] M. E. Peskin and T. Takeuchi, *Phys. Rev. D* **46**, 381 (1992).
- [96] W. Grimus, L. Lavoura, O. M. Ogreid, and P. Osland, *Nucl. Phys. B* **801**, 81 (2008).
- [97] I. Maksymyk, C. P. Burgess, and D. London, *Phys. Rev. D* **50**, 529 (1994).
- [98] C. P. Burgess, S. Godfrey, H. König, D. London, and I. Maksymyk, *Phys. Rev. D* **49**, 6115 (1994).
- [99] W. Altmannshofer, S. Gori, M. Pospelov, and I. Yavin, *Phys. Rev. Lett.* **113**, 091801 (2014).
- [100] S. R. Mishra *et al.* (CCFR Collaboration), *Phys. Rev. Lett.* **66**, 3117 (1991).
- [101] J. P. Lees *et al.* (BABAR Collaboration), *Phys. Rev. D* **94**, 011102 (2016).
- [102] D. de Florian *et al.* (LHC Higgs Cross Section Working Group), [arXiv:1610.07922](https://arxiv.org/abs/1610.07922).
- [103] R. L. Workman *et al.* (Particle Data Group), *Prog. Theor. Exp. Phys.* **2022**, 083C01 (2022).
- [104] B. Holdom, *Phys. Lett.* **166B**, 196 (1986).

- [105] I. Adachi *et al.* (Belle-II Collaboration), *Phys. Rev. Lett.* **130**, 181803 (2023).
- [106] A. M. Sirunyan *et al.* (CMS Collaboration), *Phys. Lett. B* **819**, 136446 (2021).
- [107] G. Aad *et al.* (ATLAS Collaboration), *J. High Energy Phys.* 06 (2021) 179.
- [108] D. Aristizabal Sierra, J. Liao, and D. Marfatia, *J. High Energy Phys.* 06 (2019) 141.
- [109] K. Scholberg (COHERENT Collaboration), *Proc. Sci. NuFact2017* (**2018**) 020 [arXiv:1801.05546].
- [110] J. de Blas, M. Pierini, L. Reina, and L. Silvestrini, *Phys. Rev. Lett.* **129**, 271801 (2022).
- [111] S. Banerjee, *Universe* **8**, 480 (2022).
- [112] G. Aad *et al.* (ATLAS Collaboration), *J. High Energy Phys.* 08 (2022) 104.
- [113] I. Caprini, L. Lellouch, and M. Neubert, *Nucl. Phys.* **B530**, 153 (1998).
- [114] M. Neubert, *Nucl. Phys.* **B371**, 149 (1992).
- [115] A. F. Falk and M. Neubert, *Phys. Rev. D* **47**, 2965 (1993).